THE UNIVERSITY of ADELAIDE

A study of supersymmetric decaying dark matter models

Meera Deshpande

Supervisors:
Prof. Anthony G. Williams
Prof. Martin J. White

A thesis submitted towards the degree of Master of Philosophy

The Faculty of Sciences Engineering and Technology
The University of Adelaide

May 22, 2023

For Manu and Mischa

Abstract

The current cosmological model, ΛCDM, has made many successful predictions about the Universe including the statistics of weak gravitational lensing, the existence of the baryon acoustic oscillations, and the cosmic microwave background and its angular power spectrum. However, recent observations of the Universe have challenged the model's validity and revealed many discrepancies in its parameters. Two such widely researched cosmological tensions are the Hubble and Sigma-8 (S_8) tension. While the Hubble tension is associated with the expansion rate of the Universe, the S_8 parameter quantifies the amplitude of its matter fluctuations. Measurements of weak gravitational lensing at low redshifts (late Universe) prefer weaker matter clustering amplitude than the measurements derived from the cosmic microwave background, leading to cosmological tension. Such cosmological anomalies have motivated studies into decaying dark matter and the role of new particles called SuperWIMPs (SWIMPs) for tension resolutions. The decay of a cold dark matter particle into a massive warm dark matter and a massless dark radiation decay product has been shown to resolve the S_8 tension. In this work, we build on this dark matter model by proposing a two-step decaying dark matter scenario resulting from the interplay between the Standard Model particles and supersymmetric dark matter candidates to resolve the S_8 and H_0 tension.

For the first decay, we consider a parent cold dark matter particle (SWIMP) and radiation, with significant energy injected into the Universe. Later, as the second decay, the SWIMP further decays into massive warm dark matter and massless dark radiation daughter particles. This decay causes a suppression of the power spectrum and decreases S_8 at lower redshifts. As a result, this decay model can provide a mechanism for resolving the S_8 tension. Accompanying this framework, we modified

a publicly available Boltzmann code, CLASS, to handle the complex decays primarily parametrized by decay parameters such as the decay width, the fraction of parent dark matter decay, and energy released into the plasma.

As SWIMPs are super-weakly interacting in nature, they may be impossible to detect in the current SUSY dark matter searches in colliders and indirect/direct dark matter detection experiments. However, we successfully show that cosmological observations such as the CMB power spectrum and anisotropies can extensively probe and constrain SWIMP parameter spaces currently beyond the reach of other experiments.

This work is based on the following,

- A paper, 'Cosmological constraints on supersymmetric SWIMPs,' soon to be submitted to arxiv.
- Modified version of CLASS to handle our two-step dark matter decay model, which can be found at GitHub: git@github.com:astrogirl1/ddmpy.git.

Declaration

I certify that this work contains no material which has been accepted for the award of any other degree or diploma in my name, in any university or other tertiary institution and, to the best of my knowledge and belief, contains no material previously published or written by another person, except where due reference has been made in the text. In addition, I certify that no part of this work will, in the future, be used in a submission in my name, for any other degree or diploma in any university or other tertiary institution without the prior approval of the University of Adelaide and where applicable, any partner institution responsible for the joint award of this degree. I give permission for the digital version of my thesis to be made available on the web, via the University's digital research repository, the Library Search and also through web search engines, unless permission has been granted by the University to restrict access for a period of time. I acknowledge the support I have received for my research through the provision of an Australian Government Research Training Program Scholarship.

Meera Deshpande

Acknowledgements

I want to express my deepest gratitude to my supervisors, Prof. Anthony Williams and Prof. Martin White, without whom I could not have completed such an exciting and challenging project. I am grateful for your invaluable knowledge and support over the last two years, especially through the pandemic.

Words cannot express my gratitude to Dr. Dipan Sengupta for his invaluable wisdom, patience, and guidance. He has provided incredible support and constructive feedback and pushed me through rough patches on multiple occasions. Without him and my supervisors, this project would be months off finishing. Along with them, I would like to extend my sincere thanks to Dr. Jan Hamman and Assoc. Prof. Yvonne Wong from UNSW Sydney. Their indispensable expertise in cosmology and CMB physics was extremely helpful. I know this project was no short of technical problems, setbacks, and issues, but their patience and support helped me push it to completion. Special thanks to Sharon and Silvana of the CSSM department admin team for always being friendly and extremely helpful with any matters.

I am grateful for the company of many wonderful people at the university who made this journey an exciting time in my life. From interesting physics discussions to fun banter and camping trips, you have made my time here unforgettable. Your programming help, crafternoons, coffee chats, and officeball games kept my spirits high during this process. I am thankful for my friends Melissa and Aayush for always being there through the ups and downs I've faced over the last few years.

Most importantly, I want to thank my family, Aai, Baba, and Manu, for their unconditional love and support. I am incredibly grateful for the patience and encouragement you have provided me to pursue my interests and realize my full potential. Thank you for giving me a world full of opportunities. Finally, I would like to extend the most loving thank you to my partner Mischa for your endless love and support, without which this project would not have been possible.

Contents

List of figures

List of tables

Introduction

Recent technological advancements have provided much observational data from the Universe's far reaches, leading to a high-precision, testable theory of its origins. Although the study of the Universe dates back approximately $20,000$ years, the seeds for modern cosmology were sown after Einstein proposed the theory of general relativity [16]. It later led to the development of the Friedmann equations based on the cosmological principle. One of the significant contributions to modern cosmology was by Penzias and Wilson [17] with their discovery of the Cosmic Microwave Background (CMB) signal. It was a notable discovery because it provided evidence for the Big Bang model of the Universe and what it is made of. Since then, several ground and satellite-based experiments have investigated this signal in detail, providing foundational knowledge regarding the formation of large-scale structures in the Universe. Numerous observations such as gravitational lensing, have confirmed the existence of dark matter, but it has yet to reveal its physical secrets. We now know its existence plays an essential role throughout the evolution of the Universe, especially in the formation of large-scale structures. It has become an integral part of the standard model that describes the Universe, the ΛCDM - Lambda Cold Dark Matter model. It was only after the discovery that the Universe's expansion was accelerating that the ΛCDM model became a widely established paradigm of cosmology.

In recent decades, experiments such as WMAP [18], Planck [12], SH0ES [19], and the Hubble Space Telescope Key Project [20] have come to prominence by making precise measurements of observables of the ΛCDM model at different epochs. Increased precision in observations has revealed that the ΛCDM model may not be globally consistent throughout the evolution of the Universe. One of the most interesting and notable cosmological tensions involves the Hubble parameter, which is related to the Universe's rate of expansion. The early-time value of the Hubble parameter inferred by Planck is $H_0 = 67.27 \pm 0.60\,\mathrm{km\,s^{-1}\,Mpc^{-1}}$ [12], which is currently at around $3-5\sigma$ disagreement with the local value measured by SH0ES, $H_0 = 74.3 \pm 2.2\,\mathrm{km\,s^{-1}\,Mpc^{-1}}$ [21]. Although the late-time H_0 value from the Hubble Space Telescope Key Project,

$H_0 = 74.3 \pm 2.2\,\mathrm{km\,s^{-1}\,Mpc^{-1}}$, is in agreement with SH0ES, it has reinforced the tension with Planck [22].

In addition to the H_0 tension, the parameter for the matter density, σ_8, often written as $S_8 \equiv \sigma_8\sqrt{\Omega_m/0.3}$, is also a subject of discrepancy. The S_8 depends on the Ω_m parameter, which specifies the fractional energy density of all forms of matter. The growth rate for structure in the Universe given by $f = [\Omega_m]^{0.55}$ is measured by current galaxy redshift space distortions, which in turn determines the S_8 value. Planck's model inferred parameter value for S_8 is 0.834 ± 0.016, which is higher than the present-time measurements [12]. However, the recently reported cosmic shear value from the KiDS-1000 experiment is $S_8 = 0.766^{+0.020}_{-0.014}$, which has pushed the tension to $\sim 3\sigma$ [23].

Such tensions indicate the need for possible revision of the ΛCDM model, whether as extensions or unmodelled systematic effects [24]. The S_8 and the H_0 tensions may be correlated, but current literature only proposes solutions for resolving them one at a time. For instance, the late-time measurements of a higher H_0 value prefer a lower Ω_m value which modifies the growth rate of structure parameters and the CMB anisotropies. Consequently, this induces a higher σ_8 value that disagrees with any early time measurements such as Planck. As a result, due to mutual correlations and effects, it is evident that any analysis conducted in an attempt to resolve these tensions should be conjoined and performed with a full range of data and parameters [23].

Due to the vastness and unknownness of the dark sector, many models containing different properties of dark matter, dark energy, and dark radiation have been explored as possible solutions to the tensions. The wide range of experiments now available to study the early Universe provides constraints on the observables of ΛCDM parameters while allowing room for modifications to parameters that may alleviate tensions. For instance, decaying dark matter (DDM) theories have become increasingly popular. Based on the substantial presence of cold dark matter today, it has to be approximately stable on the overall timescale of our Universe. However, it is reasonable to predict that it decays with a long lifetime or that it decays into other dark sector particles within the agreement of measurements. Moreover, suppose decaying dark matter has a lifetime shorter than the age of the Universe. In that case, its signatures may show up in the observations of the early Universe, such as in the CMB anisotropies.

Joining the quest to find a resolution, this work assesses the phenomenology of a two-step decaying dark matter model, where the decay products of the first decay are a CDM particle and a photon, and of the second decay is a massive WDM particle with

a massless dark radiation (DR) component. For the first decay, we consider a weakly interacting massive particle (WIMP) as the mother CDM particle and a super-weakly interacting massive particle (SWIMP) as the daughter dark matter particle. As discussed by Feng et al. in Ref. [25] a WIMP $\rightarrow$ SWIMP $+\gamma$ decay scenario conforms to constraints introduced by measurements of the CMB and matches the WIMP relic density observed today. This makes the SWIMP an ideal dark matter candidate, and this model a well-motivated theory. Later in the Universe's evolution, the SWIMP decays into another set of massive and massless dark matter products, forming the second decay step in our model. The two-step decay allows more control over the decay parameters of the ΛDDM model that affect the base parameters of ΛCDM. For the decay scenarios, we will consider two well-motivated supersymmetric dark matter candidates, the neutralino as the WIMP and the gravitino as the SWIMP.

The gravitino can be a SWIMP and viable dark matter candidate depending on the supersymmetry breaking mechanism. It weakly interacts with Planck-scale suppressed interactions and has promising prospects for experimental detection. In the supersymmetric model, the gravitino can be produced either thermally or non-thermally. The thermal production of gravitinos occurs due to scattering processes in the hot plasma after inflation. As a result, the relic density of gravitinos depends on the reheating temperature and can exceed the critical density if gravitinos are heavier than $\mathcal{O}$(keV). In addition, unstable gravitinos can also affect primordial nucleosynthesis, which can disagree with predictions of the big bang nucleosynthesis (BBN). Hence, the BBN can provide strong constraints on the reheating temperature and, consequently, the gravitino number density [26].

Alternatively, the gravitino abundance can also be contributed via decays of heavier supersymmetric particles via non-thermal processes. Gravitinos produced non-thermally can be unstable but have decay lifetimes comparable to the age of the Universe, making them stable enough to account for the dark matter abundance measured today. However, as the dark matter density in the Universe is more significant than ordinary matter, if the gravitinos decay in the late Universe, the decay signal could be strong enough to be observed in the astrophysical signals or the CMB signatures [27]. In this thesis, we primarily focus on the interplay between the Standard Model particles and supersymmetric decaying dark matter models with exotic energy injections during different epochs of the Universe involving gravitino and neutralino decay properties. Building on the framework described in ref [28, 29] and [30] for a ΛDDM model (Lambda Decaying Dark Matter), we investigate a parent neutralino (primarily a bino, $\tilde{B}$) decaying into a gravitino ($\tilde{G}$)

and a photon in the first decay; and for the second decay at a later time, the gravitino decaying into a sneutrino (warm dark matter) and neutrino (dark radiation).

As an integral part of this research work, we modified the Boltzmann code - CLASS [31] to investigate our proposed decay models. We merged two different versions of CLASS, ExoCLASS [31] to handle the first, WIMP decay and `class_decays` to handle the second, WDM decay [32]. Currently, multiple codes are built to investigate exotic energy injections and their effects on the CMB spectra. Codes such as DarkHistory [33], and CosmoTherm [34] include the processes of energy injection in the early Universe through dark matter decay/annihilation but are limited to arbitrary standard model particles as decay products and simple decaying dark matter scenarios. The code developed as a part of this project contributes to the ability to handle complex decay scenarios. It includes multiple alternatives for decay products such as neutrinos, warm dark matter, cold dark matter, and dark radiation. Using our code, we investigate constraints on the gravitino mass ($m_{\tilde{G}}$), specifically in the neutralino to gravitino decay model, where $m_{\tilde{G}}$ affects the lifetime and decay fraction of the neutralino. We present foundational work that we will extend in the future to investigate if our energy injection scenarios could resolve the H_0 and S_8 cosmological tensions.

The structure of the thesis is as follows,

- The study of dark matter is an interdisciplinary field. In Chapter 1, we introduce the standard model of particle physics and its supersymmetric extension and discuss the characteristics of the gravitino.
- In Chapter 2, we discuss the key events in the Universe's history and present background information on its contents as a foundation to understand better the effects of energy injection presented later in the thesis.
- Chapter 3 presents the ΛCDM model and definitions of quantities that parametrize the geometry of the Universe. We list the most recent model-inferred values for the six fundamental parameters of the ΛCDM model and discuss the importance of the cosmic microwave background power spectra.
- In Chapter 4, we provide in-depth insight into our two-step decaying dark matter model, including the steps taken to produce our proposed code and to test and verify it.
- In Chapter 5, we discuss the physics of the decay models specific to the neutralino and gravitino cases and present the results of the mass constraints on the SWIMPs.

Chapter 1

The Standard Model and Beyond-Standard-Model

The discovery of the electron in 1892 marked the birth of modern particle physics. The existence of protons and neutrons inside the atom was revealed through extensive nuclear experimentation, which sparked the search for other particles. Since then, particle physics has evolved to describe the forces and interactions of particles at the most elementary level. The Standard Model (SM) is a remarkable theoretical framework built from observations and measurements that outlines all the existing knowledge of particle behavior. To study physics beyond the Standard Model, it is necessary to understand what it offers [35]. This section summarises the Standard Model and briefly introduces its supersymmetric extension.

1.1 Standard Model Forces and Particles

The Standard Model aims to describe a unified theory of matter with the strong, the weak, and the electromagnetic (EM) forces in the language of gauge-field theories. Particle physicists have characterized nature into four distinct forces depending on their effective ranges and strengths measured at an energy value of 1 GeV. The strong nuclear force has a range of 10^{-15} m, whereas the weak force, responsible for radio-active decay, has a range of 10^{-17} m. The electromagnetic (EM) force that acts between charged particles has an extremely long range. The Standard Model combines the electromagnetic and the weak forces to create a unified electroweak (EW) gauge theory. On the other hand, gravity, the

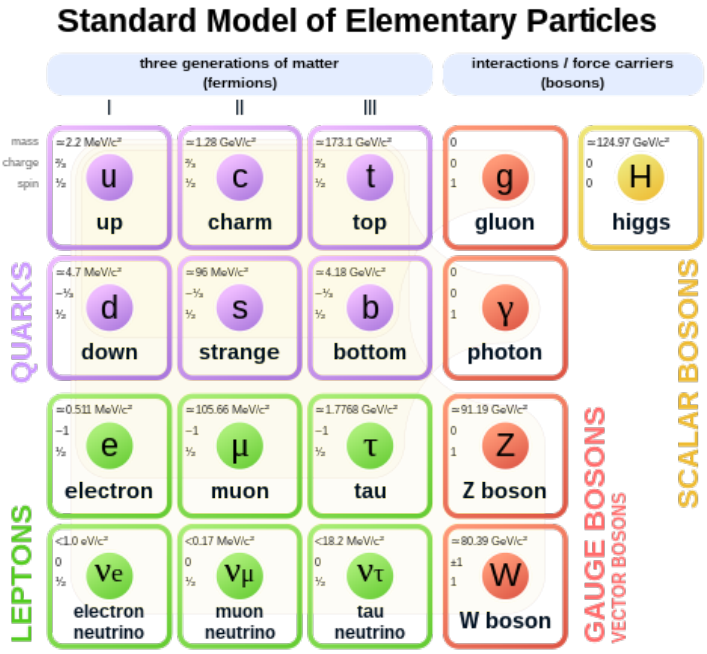

Figure 1.1 A summary of the Standard Model particles and forces [1]

fourth force, also has a long-range but a low-energy coupling constant $\sim 10^{-38}$, which makes it too weak to be observed in particle accelerator experiments [36].

Particles of the Standard Model are characterized using quantum numbers corresponding to gauge symmetries, which are represented by the group $SU(3)_C \times SU(2)_L \times U(1)_Y$. The C stands for color, L is related to left-handedness and chirality, and Y denotes hypercharge. The $SU(2)_L \times U(1)_Y$ symmetry group describes the electroweak interactions between subatomic particles. The $SU(3)_C$ group represents the strong interactions that act on quarks of associated color charges, termed the Quantum Chromodynamics (QCD). This strong interaction is not involved in electroweak symmetry breaking and remains a symmetry at all energies. However, the Brout-Englert-Higgs mechanism breaks $SU(2)_L \times U(1)_Y$ into $U(1)_Q$, generating the photon, three weak force carriers W^+, W^- and Z^0, and a Higgs boson.

Figure 1.1 summarizes the full particle content of the SM, including information on their charge, mass, and spin. These fundamental particles are divided into subgroups, namely fermions that have spin-1/2 and obey Fermi-Dirac statistics and bosons (gauge bosons) with spin one that obeys Bose-Einstein statistics. The fermions are further organized into three generations with different masses and are divided into leptons and quarks. The leptons are the electron, muon, and tau, each with corresponding massless

and neutral neutrinos. One of the shortcomings of the Standard Model is that it predicts neutrinos to be massless, in contradiction with experimental observations. Still, extending the SM to account for neutrino masses and mixing is straightforward: introducing the lepton PMNS matrix (Pontecorvo-Maki-Nakagawa-Sakata) [37, 38].

The quarks are constituents of nucleons and are further split into up-type and down-type quarks. The quarks carry a fractional electric charge and are classified into three generations, similar to leptons. The up-type quarks are up, charm, and top, and the down-type quarks are down, bottom, and strange. Quarks interact via the strong, weak and electromagnetic forces. For each fermion, the SM also predicts the existence of a corresponding anti-matter particle with an opposite charge. Each member of a lepton or quark generation has a more significant mass than the corresponding lepton or quark of a lower generation [37].

The strength of the strong force gives rise to bound states of mesons, baryons and pentaquarks and the spin one gauge bosons mediate interactions among fermions. The breaking of the electroweak symmetry ($SU(2)_L \times U(1)_Y$) to the residual gauge symmetry of Quantum Electrodynamics (QED) ($U(1)_Q$) can be explained by invoking the Higgs Field. Fermions interact with the Higgs Field and acquire masses, which induces misalignment of quark mass eigenstates with respect to weak charge eigenstates. This mechanism allows the heavier fermions to decay into lighter ones [36]. The LHC program has a diverse range of experiments to test the electroweak theory. So far at the LHC and previous experiments, the electroweak sector of the Standard Model has been measured to incredible accuracy using electroweak precision tests and precision tests of the SM parameters.

1.1.1 The Standard Model Lagrangian

The particles, symmetries and interactions in the Standard Model can be encapsulated in a mathematical representation, a form that describes all the particles as discrete excitations of fields. The Lagrangian density function is written as

$$\begin{aligned}\mathcal{L}_{\text{SM}} = &-\frac{1}{4}F_{\mu\nu}F^{\mu\nu} - \frac{1}{4}G_{\mu\nu}G^{\mu\nu} + i\bar{\psi}\gamma^{\mu}D_{\mu}\psi + \\ &\bar{\psi}_i y_{ij}\psi_j + h.c. + |D_{\mu}\phi|^2 - V(\phi).\end{aligned} \tag{1.1}$$

The first $-\frac{1}{4}F_{\mu\nu}F^{\mu\nu} - \frac{1}{4}G_{\mu\nu}G^{\mu\nu}$ terms are the kinetic terms describing the interactions within the gauge fields of each of the subgroups $SU(3) \times SU(2) \times U(1)$. The next term,

$i\bar{\psi}\gamma^\mu D_\mu\psi$, encompasses the kinetic terms for the Dirac fermionic fields and the couplings of gauge fields to fermions, also accounting for interactions. The Yukawa coupling represented by $\bar{\psi}_i y_{ij}\psi_j$ and its Hermitian conjugate $h.c$, gives fermions their masses. The last two terms $|D_\mu\phi|^2$ and $V(\phi)$ govern the self-interaction of the Higgs boson and the Higgs potential, which leads to electroweak symmetry breaking [39].

1.2 Higgs and the Hierarchy Problem

How do the subatomic particles in the Standard Model acquire their mass? This question intrigued scientists until, in 1964, Peter Higgs, Robert Brout and Francois Englert formulated a mechanism that explained the mass of particles [40, 41]. Suitably named the Brout-Englert-Higgs mechanism, it introduces a scalar potential - the Higgs Field, which exists at all points in space. The field's vacuum expectation value (vev) at high energies is zero. However, at low background energies, such as the present Universe, the vacuum expectation value of the field is non-zero. For particles interacting with this field, this means they acquire non-zero masses [26].

The Lagrangian density of the Higgs field and its potential can be written as the following

$$\mathcal{L}_H = \frac{1}{2}(D^\mu\Phi)^\dagger(D_\mu\Phi) - V(\Phi), \tag{1.2}$$

$$V(\Phi) = \mu^2\Phi^\dagger\Phi + \lambda(\Phi^\dagger\Phi)^2, \tag{1.3}$$

where μ^2 is connected to the negative of the Higgs' mass parameter and λ is the Higgs field self-coupling parameter [42].

In 2012, the Higgs boson was discovered with a mass of 125 GeV at the LHC. The discovery implies that in the Eq. (1.3), $\lambda = 0.126$ and $m_H^2 = -(92.9)\,\text{GeV}^2$. However, every direct or indirect particle coupling to the field in the Standard Model contributes quantum corrections to m_H^2. For instance, given a fermion f of mass m_f then the Feynman diagram yields a correction like follows,

$$\Delta m_H^2 = -\frac{|\lambda_f|^2}{8\pi^2}\Lambda_{UV}^2 + ... \tag{1.4}$$

And for a boson coupling to the Higgs field, i.e. a scalar particle of mass m_s, Eq. (1.4) changes to look like,

$$\Delta m_H^2 = \frac{\lambda_S}{16\pi^2}\left[\Lambda_{UV}^2 - 2m_s^2 \ln\left(\frac{\Lambda_{UV}}{m_S}\right) + ...\right] \tag{1.5}$$

The Λ_{UV}^2 term represents a cutoff of the energy scale at which new physics should enter to alter the high-energy behaviour of the Standard Model. When calculating these radiative corrections to the Higgs mass, the loop contributions add quadratically divergent terms around the Λ_{UV} cut-off scale. If this scale is chosen to be the same order of magnitude as the Planck scale 10^{18} GeV, corrections to the Higgs mass would need to be fine-tuned to the order 10^{-30} to obtain the required value of m_H^2 as experimentally measured. Theoretically, this calculation makes the Higgs mass significantly smaller than the grand unification scale. This discrepancy is named the gauge hierarchy problem [26, 35].

It is believed that cancellations of high order contributions can only be achieved through a symmetry. The fermionic and bosonic loop contributions to the Higgs mass, as in Eq. (1.4) and Eq. (1.5) are of opposite signs. Hence, a potential symmetry needs to relate bosons and fermions to account for loop cancellations. Introducing supersymmetry! Supersymmetry (SUSY) attempts to solve the hierarchy problem by introducing two bosonic superpartners for every SM fermion and a fermionic superpartner for every SM boson. Assuming SUSY is an exact symmetry, these extra contributions cancel the quadratically divergent terms in calculating the Higgs mass [26].

The discovery of the Higgs boson has given rise to one of the most striking conclusions: the current experimental value for the Higgs mass poses a possibility of the existence of a metastable electroweak vacuum if beyond-Standard-Model physics is not considered. The metastability of the Higgs vacuum is significant for cosmology as mulitple mechanisms could have triggered the decay of the electroweak vacuum in the early Universe [43].

1.3 Supersymmetry

Although well-tested and established, the Standard Model is still a work in progress and cannot fully explain all the known physics phenomena. The hierarchy problem, properties of dark matter, and the matter-antimatter inequality in the Universe are some of the significant problems that have motivated the emergence of the beyond-standard-model symmetries and theories. One of these popular theories is supersymmetry (SUSY),

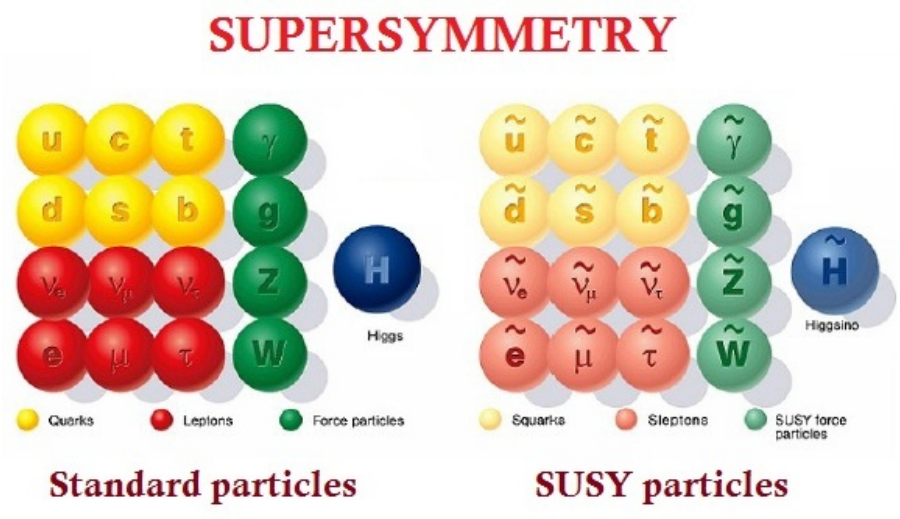

Figure 1.2 A summary of the supersymmetric particles and forces [2]

and its smallest addition of predicted SUSY particles to the SM is named the Minimal Supersymmetric Standard Model (MSSM) [35]. SUSY is a symmetry between fermions and bosons that turns a bosonic state into a fermionic state and vice versa. In other words, it transforms bosons with integer spins into fermions of half-spins and fermions to bosons with integer spins. [26].

1.3.1 Particle Content of the MSSM

The MSSM consists of both matter/scalar and gauge/vector supermultiplets. In this extension of the SM, each of the fundamental particles is in either a scalar or a gauge supermultiplet and must have a superpartner with a spin differing by 1/2 units [26]. The superpartners of the SM fermions are known as scalar fermions, and the formal SUSY names are prepended with 's', for example, 'sfermions', with 'squarks' and 'sleptons'. The superpartner names of SM bosons are suffixed with '-ino' [44]. The particle symbols are often written with a tilde to denote that they are superpartners. The vector bosons of the SM inhabit the MSSM gauge supermultiplet, and their fermionic superpartners are called gauginos. The gauge supermultiplets contain $\hat{G}$, which consists of gluons and their superpartners, $\hat{W}$ which corresponds to electroweak bosons and their superpartners 'winos', and $\hat{B}$ which corresponds to the gauge boson and its superpartner, 'bino' ($\tilde{B}$). The chiral supermultiplets contain all the pairs of fermions of the SM as well as their superpartners [35].

1.4 Particle Candidates for Dark Matter

The existence of dark matter is well-motivated by astronomical and physical evidence obtained over the last century [45, 46]. Studying the Standard Model and its extensions has provided many particle candidates for dark matter. A particular class of dark matter candidates is that of the Weakly Interacting Massive Particles (WIMPs). They have acquired such a name because they do not interact strongly with other matter and are electrically neutral. Historically, neutrinos of the Standard Model were considered dark matter candidates because compared to other particles; they are relatively stable, weakly interacting and electrically neutral. Nevertheless, they have been eliminated due to their relativistic nature; a neutrino-dominated Universe would have exhibited a different formation of large-scale structure to what has been astrophysically observed [47].

1.4.1 SUSY Dark Matter Candidates

Symmetries governing the SM guarantee that baryon and lepton numbers are conserved, which inhibits proton decay. SUSY conserves such a symmetry, 'R-Parity' or 'matter-parity' states that protons or other lightest baryons cannot decay quickly to other particles via the exchange of SUSY particles. This also prevents the decay of the lightest supersymmetric particle (LSP) into SM particles, making it stable and an ideal candidate for dark matter [47]. The MSSM has several possible particle candidates that can be dark matter. The most popular candidate of the WIMP class is the neutralino - a superposition of the higgsinos and electroweak gaugino bosons [47, 48]. The gravitino, the superpartner of the graviton, is also considered a fit candidate for dark matter, whose mass depends on the SUSY breaking scale. All of these particles are weakly interacting and electrically neutral, satisfying the condition to be WIMP dark matter [47]. In this work, we investigate a specific decay scenario of the neutralino as the WIMP and the gravitino as the SWIMP.

Figure 1.3 shows a summary of the particle candidates, and classes of dark matter for typical mass ranges [49, 50].

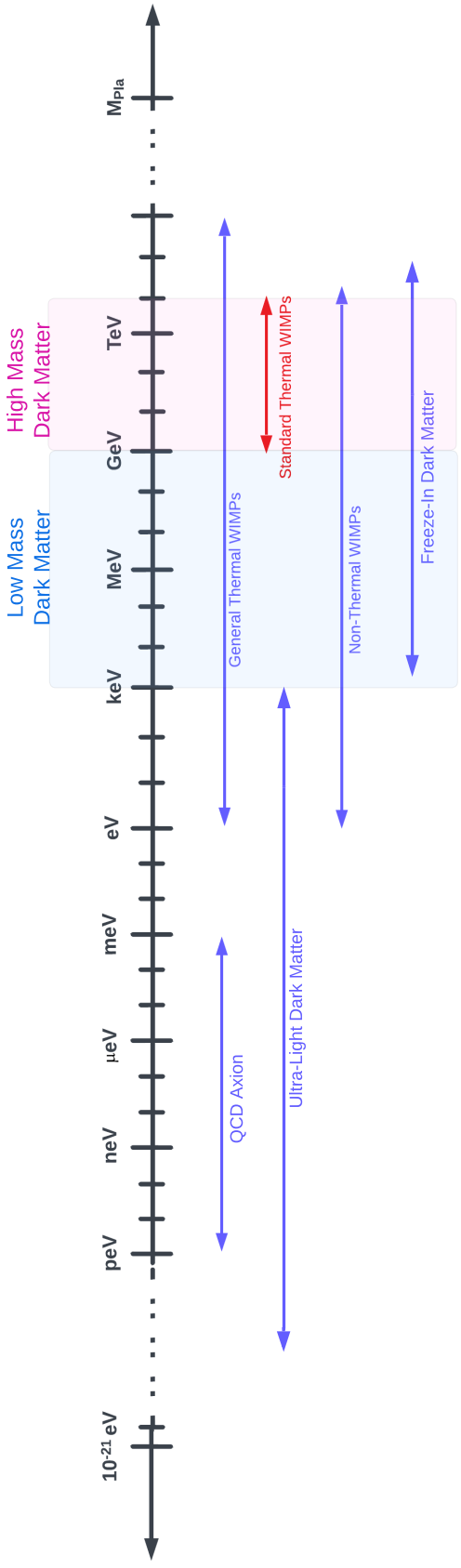

Figure 1.3 A summary of particle candidates and classes for dark matter. Diagram inspired by Ref. [3,4]

1.5 Gravitino Cosmology

Gravitinos have Planck-scale suppressed interactions, but a rich phenomenology that complements neutralino cosmology well and has many implications for cosmology. The following section introduces some gravitino properties necessary for formulating gravitino decay models.

1.5.1 Gravitino Mass

Supersymmetry breaking enabled by soft parameters can explain the mass difference between the Standard Model particles and their superpartners. To prevent the reintroduction of undesired quadratic or logarithmic divergences in the supersymmetric Lagrangian, the term "soft" is utilized to describe the parameters of supersymmetry-breaking. However, there is currently no model that can fully explain a SUSY-breaking mechanism via particle interactions of the MSSM. Hence, a hidden sector must exist where SUSY is broken, whose effects can be mediated to the visible sector via suppressed interactions.

The supergravity theory posits that the spin-2 graviton has a fermionic superpartner known as the spin-3/2 gravitino, which possesses an odd parity value ($R = -1$). The gravitino is regarded as the gauge field of local supersymmetric transformations, and both the gravitino and the graviton are massless in the absence of supersymmetry breaking. In accordance with the super-Higgs symmetry, which generates fermionic SUSY generators, the breaking of supersymmetry leads to the creation of a fermion called the goldstino. Similarly to the Higgs mechanism in the Standard Model, which allows the $W^{\pm}$ and Z bosons to gain mass through the absorption of Nambu-Goldstone bosons resulting from the electroweak symmetry breaking, the Lagrangian of supergravity features a mixing term between the gravitino and the goldstino. As a result, once supersymmetry is broken, the gravitino acquires mass by absorbing the goldstino [26], and the resulting mass is expressed as

$$m_{3/2} = \frac{\mathrm{F}}{\mathrm{M_{Pl}}}. \tag{1.6}$$

Here, F is the vacuum expectation value of the hidden field that causes the symmetry breaking and $\mathrm{M_{Pl}}$ is the Planck mass (of the order $\sim 10^{18}\,\mathrm{GeV}$). The two well-known symmetry-breaking mechanisms are gravity-mediated (Planck-mediated) and gauge-

mediated, which give distinctly different predictions for the SUSY breaking scale and consequently the gravitino mass.

- The **Gravity-Mediation** mechanism for SUSY breaking assumes that SUSY is broken spontaneously in the hidden sector by a vev $\langle \mathrm{F} \rangle$, then soft parameters in the visible sector are expected to be the order of

$$m_{\text{soft}} \sim \frac{\langle \mathrm{F} \rangle}{\mathrm{M_{Pl}}} \sim m_{3/2}, \tag{1.7}$$

  where the soft masses vanish in the limits $\langle \mathrm{F} \rangle \to 0$ or $\mathrm{M_{Pl}} \to \infty$. For an m_{soft} value around the TeV scale, the scale of supersymmetry breaking in the hidden sector is around $\sqrt{\langle \mathrm{F} \rangle} \sim 10^{10-11}\,\mathrm{GeV}$.

- However, the **Gauge-Mediation** mechanism consists of messenger particles that couple to MSSM particles through gauge interactions and mediate the breaking of supersymmetry to the visible sector. Then, a similar estimation for the mass of the soft terms can be given as

$$m_{\text{soft}} \sim \frac{\alpha_a}{4\pi} \frac{\langle \mathrm{F} \rangle}{\mathrm{M_{messenger}}} \sim m_{3/2}, \tag{1.8}$$

  where the $\alpha_a/4\pi$ term is related to the loop factor for the Feynman diagrams of the gauge interactions and $\mathrm{M_{messenger}}$ is the scale of the masses of the messenger fields. Assuming $\mathrm{M_{messenger}}$ and $\langle \mathrm{F} \rangle$ are of similar magnitudes, then the scale of supersymmetry breaking can be around $\sqrt{\langle \mathrm{F} \rangle} \sim 10^4\,\mathrm{GeV}$, much lower than the gravity-mediated case [26].

The gravitino's interactions in a gravity-mediated SUSY breaking model are of gravitational strengths and its mass is comparable to MSSM sparticles around and above 100 GeV. On the other hand, the gauge-mediated supersymmetry breaking model predicts that the gravitino is much lighter than the MSSM sparticles that will eventually decay into products containing it. This mechanism can make the gravitino an ideal dark matter candidate in certain scenarios [26].

1.5.2 Production of Gravitinos

The main production mechanisms for gravitinos involve thermal and non-thermal processes. At the end of inflation, gravitinos can be produced in thermal scattering processes

in the hot plasma after reheating of the Universe. The relic density [1] of gravitinos is then dependent on the reheating temperature (T_R) and gluino mass ($m_{\tilde{g}}$) [51]

$$\Omega_{3/2}h^2 \simeq 0.27\left(\frac{T_R}{10^{10}\,\mathrm{GeV}}\right)\left(\frac{100\,\mathrm{GeV}}{m_{3/2}}\right)\left(\frac{m_{\tilde{g}}}{1\,\mathrm{TeV}}\right)^2. \tag{1.9}$$

If the gravitino is stable and not lighter than a few keV, its abundance can exceed the critical density of the Universe. However, if thermally produced gravitinos are unstable, their decay products and energy injection may affect the light element abundances and cause disagreement with big bang nucleosynthesis (BBN) predictions. This condition allows the BBN to provide strong constraints on the reheating temperature and consequently on the mass of the gravitino, ensuring gravitino physics does not disturb the critical density of the Universe [51–53].

In the non-thermal production scenario (production through late decays), as the gravitino interacts only gravitationally and has its interactions Planck-scale suppressed, it is assumed to have negligible effects on the thermodynamics of the early Universe. The neutralino freezes out as a usual weakly-interacting dark matter in the early Universe with an acceptable relic density value. At a later time given by Eq. (1.10), it decays to the gravitino [51],

$$\tau \sim \frac{M_*^2}{M_{\mathrm{weak}}^3} \sim 10^5 - 10^8\mathrm{s}, \tag{1.10}$$

where $M_* = (8\pi G_N)^{-1/2} \approxeq 8.4 \times 10^{18}$GeV is the reduced Planck Mass and M_{weak} refers to the mass scale associated with the weak force [51].

The gravitino relic density, inherited from the WIMP relic density, can then be given as

$$\Omega_{\tilde{G}} = \frac{m_{\tilde{G}}}{m_{\mathrm{WIMP}}}\Omega_{\mathrm{WIMP}}. \tag{1.11}$$

According to high-scale supersymmetry-breaking theories, the neutralino and the gravitino masses are of the same order. Consequently, the gravitino will not have enough kinetic energy to increase the reheating temperature, preventing any perturbations to BBN predictions and thus satisfying BBN constraints. In addition, the gravitinos have

[1] The term "relic density" refers to the abundance of stable particles remaining in the universe after a process of freeze-out, in which they are no longer in thermal equilibrium with the cosmic background radiation. This is explained in detail in Chapter 2.

Planck-suppressed interactions. They are long-lived, with decay lifetimes comparable to the age of the Universe, which can explain the large dark matter abundance measured today.

The decay signals from the neutralino decay, $\tilde{\mathrm{N}} \rightarrow \tilde{\mathrm{G}} + \mathrm{S}$, are observable through the production of an SM particle, S and its electromagnetic cascades in the early Universe. In addition, the decay signals only depend on the lifetime of the neutralino in our case and the fraction of energy released in the decay. This will be discussed in detail in the following chapters.

Status of SUSY at collider experiments

Supersymmetry is one of the most popular physics theories, and evidence for it is being widely searched for in experiments at the LHC, such as ATLAS and CMS. For example, the Minimal Supersymmetric extension to the Standard Model (MSSM) more than doubles the number of particles of the Standard Model. In addition, if supersymmetry is imposed as a local symmetry, it includes gravity, containing the spin-2 graviton and its superpartner spin-3/2 gravitino.

The MSSM has around 126 unconstrained parameters in addition to the parameters of the Standard Model, and to search for them at collider experiments, many simplified assumptions are made. Constraints on supersymmetry have been calculated and interpreted for different models. Although simplified models do not fully represent the complex MSSM framework, they provide insight into the scales needed to probe for new physics. So far, no SUSY has been detected experimentally, but upper limits of around $1 - 2\,\mathrm{TeV}$ have been set on masses of squarks and gluinos. However, supersymmetry may be difficult to detect via strong interaction production of the gluinos and squarks pairs but could be seen through the decay of electroweak partners. Searches at the LHC rely on prompt decays of the electroweak partners with very short lifetimes.

Additionally, conditions are far less conclusive for electroweak bosons and lepton superpartners due to their small production cross-sections. Current constraints exclude slepton masses only up to a few-hundred GeV. For the electroweak bosonic superpartner masses, neutralinos, and charginos, current constraints are of the $100 - 300\,\mathrm{GeV}$ order in the MSSM [54–56].

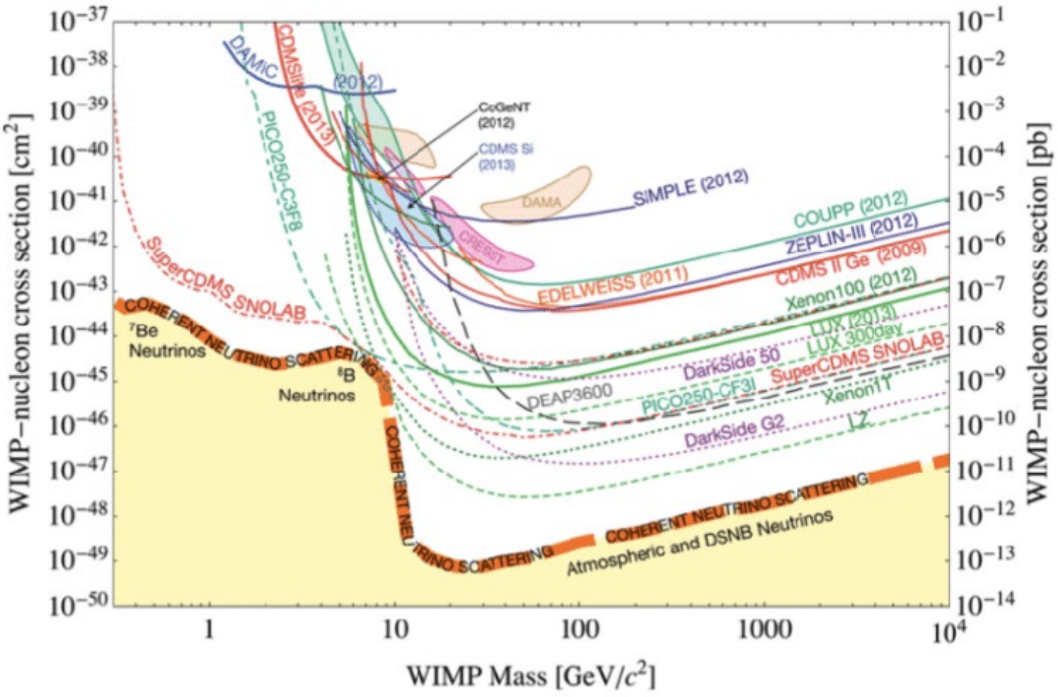

Figure 1.4 The current experimental constraints on WIMP-mass and WIMP-nucleon scattering cross sections for various experiments worldwide. Some of the detectors shown are DAMA, EDELWEISS, XENON1T, DarkSide50, DARWIN and SuperCDMS [5].

Figure 1.4 shows the current experimental exclusion regions worldwide for various dark matter detection experiments. The parts above labeled lines in the figure are considered excluded regions, and the neutrino floor is depicted as the yellow region at the bottom of the figure under the orange dashed line [5].

The neutrino floor is a hypothetical threshold in the sensitivity of neutrino detectors. As detectors improve, they become capable of detecting lower-energy neutrinos, which are more abundant in the universe. However, eventually, the detector's sensitivity is hindered by the natural background of neutrinos generated by sources like the sun and the atmosphere. This background level is called the "neutrino floor," and it sets a limit on the detector's sensitivity to low-energy neutrinos. This floor also serves as a minimum threshold for detecting weakly interacting massive particles (WIMPs) in direct dark matter experiments. When the sensitivity of a detector reaches the neutrino floor, the signals from dark matter particles become obscured by the background of neutrinos, making them difficult or impossible to detect [57, 58].

Taking the dark matter to be a WIMP, astrophysical studies of energies in the 100 TeV scale can tie into the possible new physics in the particle physics realm. Using the properties of WIMPs, the dark matter density and cross-section can be predicted, allowing comparable analyses of the microscopic predictions with astrophysical observations [59].

1.6 Summary

In this chapter, we provide background information on the Standard Model of particle physics and the motivation for supersymmetry. The key takeaways from this chapter are:

- A summary of the Standard Model of particle physics and some of its shortcomings.
- The Higgs mass and the hierarchy problem as a motivation for supersymmetry and an introduction to the minimal supersymmetric extension of the standard model.
- Supersymmetric particle candidates for decaying dark matter (DDM) and gravitino cosmology that is relevant for the DDM model presented in this thesis.

Chapter 2

Cosmology

2.1 A Brief History

Einstein's theory of general relativity has provided the most notable explanation of the evolution of the Universe. This theory has answered big questions about our existence and the evolution of the Universe and allowed testing against astronomical observations. After measurements by the Hubble telescope, several modern cosmological theories emerged stipulating that the Universe emerged about 13.7 billion years ago with a hot, dense, homogenous and isotropic distribution of matter and has been expanding and cooling since then. The theory of inflation incorporates the success of this model- the Big Bang model, which today provides the standard model of cosmology, ΛCDM. The inflation theory suggests that when the Universe was 10^{-35} s old, it expanded exponentially fast and diluted all matter, radiation, or early time structures. High temperatures accompanied this expansion; hence, no bound states could exist during this time. As the Universe expanded and cooled after this phase, the formation of atoms, protons, neutrons, molecules and thus clouds, stars, planets and other celestial masses occurred [60, 61].

The following section summarises critical events in the history of the Universe to aid in understanding how decaying dark matter models may affect its evolution.

Time: 10^{-32} s - 10^{-5} s after the Big Bang

It is theorized that inflation, the exponential expansion of the Universe, lasted from about 10^{-36} s - 10^{-12} s after the Big Bang. It is also hypothesized that baryogenesis took place sometime during this period. Baryogenesis is a physical process that may explain

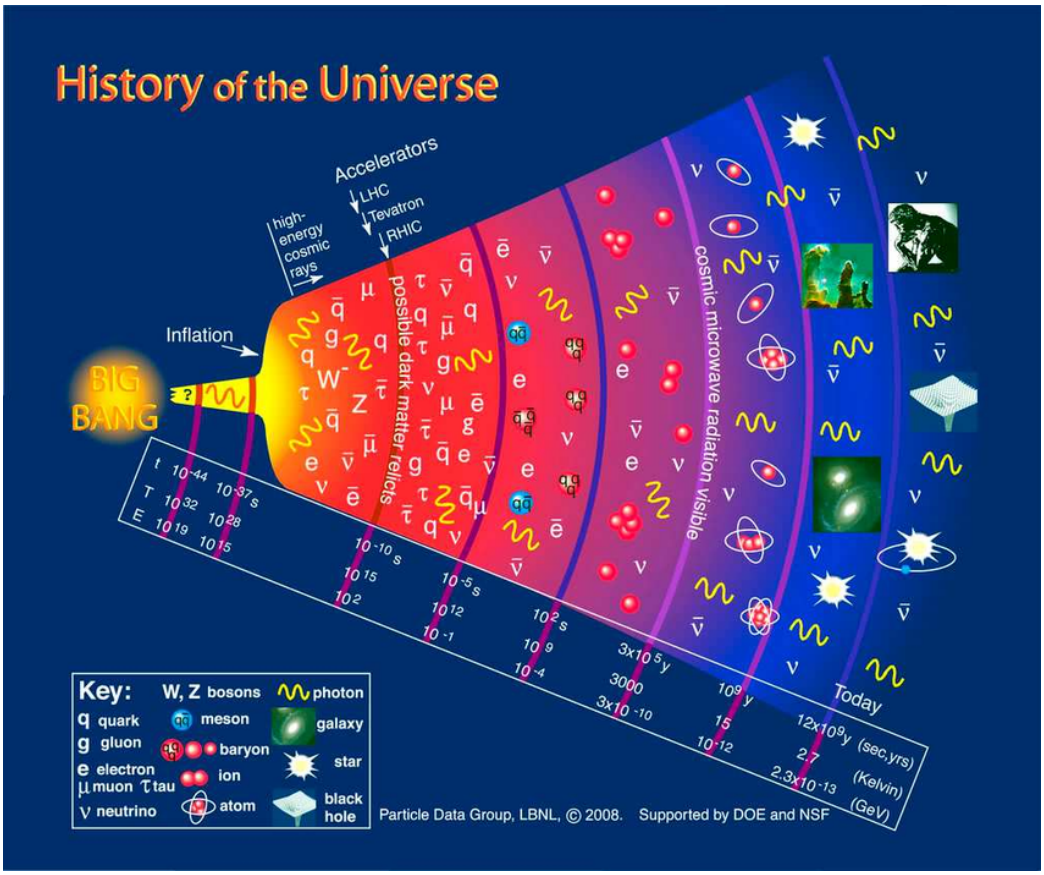

Figure 2.1 History of the Universe [6]

the baryon asymmetry in the Universe observed today, that is, the imbalance between the matter and antimatter abundance. Following this epoch, the Universe expanded more slowly as the temperature began to drop. Around 10^{-12} s, the Universe dropped to a temperature of 100 GeV and another phase transition occurred that decoupled the EM and weak forces from the EW force. As a consequence of EW symmetry breaking, all elementary particles interacting with the Higgs became massive. However, high temperatures still forbade the binding of particles. At ≈ 150 MeV, the QCD phase transition took place as the temperature dropped further, below which, strong interactions between quarks and gluons could form baryons and mesons [60, 62].

Time: 10^{-5} s - 1 s after the Big Bang

As the temperature dropped below 100 GeV, particle interactions dominated this time in the Universe.

Boltzmann Equation and Freeze Out

One of the most important quantities that describes particle interactions and densities is the reaction rate per particle (Γ),

$$\Gamma = n\langle\sigma v\rangle \tag{2.1}$$

where n is the number density of the particle, and $\langle\sigma v\rangle$ is the average of its effective annihilation cross-section multiplied by the particle's relative velocity, v. Γ provides insight into the frequency of particle interactions, which was high in the early Universe. The expansion resulted in fewer interactions. As the Universe cooled, lighter particles did not have enough kinetic energy to produce heavier particles. At a later point in time, some particle densities were too low to support frequent interactions. Such particle species fell out of thermal equilibrium with the rest of the Universe. These particle densities, comoving with the expansion have remained constant since then. This mechanism is called a 'freeze-out' and the density of a specific particle species since its freeze-out phase is called the relic density [47].

The Boltzmann equation is an expression that provides the rate of change of the number density of certain particles, dn/dt. It can be written, as in Eq. (2.2), in terms of the total time derivative of the distribution function of a particle species (i) on the left and a quantity C that describes the effects of all its interactions, including with other species.

$$\frac{Df_i}{Dt} = C[f_i] \tag{2.2}$$

In the absence of interactions, the Df_i/Dt term is equal to a non-relativistic matter conservation equation given as

$$\frac{Df_i}{Dt} \equiv \frac{dn}{dt} + 3\frac{\dot{a}}{a}n = 0. \tag{2.3}$$

Here, $H = \dot{a}/a$ is the Hubble parameter, which will be discussed in detail in the next chapter. The right-side of Eq. (2.2) is only significant when considering interactions. In equilibrium, the probability of forward interactions is the same as inverse interactions, such as annihilation or recombination. The rate of interactions can be given as Γn, where Γ is from Eq. (2.1), and n is the number of particles. Accounting for both forward and

inverse interaction rates and the equilibrium number density of particles n_{eq}, the total Boltzmann equation can be written as [63]

$$\frac{dn}{dt} = -3Hn - \langle\sigma v\rangle(n^2 - n_{eq}^2). \tag{2.4}$$

The $\langle\sigma v\rangle$ quantity defines the annihilation rate of particles and determines the relic densities. The relic density will be lower if a particle has a large annihilation rate. In contrast, particles with the low annihilation rates do not interact as easily and have the largest relic densities [47]. As the time and temperature depend on the type of interaction considered, the solution to this equation needs to be calculated numerically.

The integrals of the Boltzmann equation tell us how the velocity, number-density and other such quantities evolve with time. The main physical interactions during the early Universe are electron-positron annihilation, pair production or hydrogen recombination and ionization. For each interaction the Boltzmann equation takes into account the respective cross-sections and interaction rates. Hence, the solution to the Boltzmann equations gives the full description of particle density evolution and provides insight into the various physical processes in the early Universe.

Dark Matter Freeze-out

Recall that WIMP dark matter does not interact strongly with other matter and is electrically neutral. So, it is believed to have decoupled from ordinary matter quite early in the Universe. As the Universe dropped to temperatures of around $\mathcal{O}(1-10)\,\mathrm{MeV}$, the WIMPs dropped out of equilibrium with the rest of the thermal bath which is now measured as the WIMP relic density. This is known as dark matter freeze-out.

Neutrino Freeze-out

Neutrinos were in thermal equilibrium with the primordial plasma and interacted only through the weak interaction. As the rate of expansion increased, the temperature dropped, and neutrinos decoupled at around 1 s or $T \approx 1$ MeV after the Big Bang.

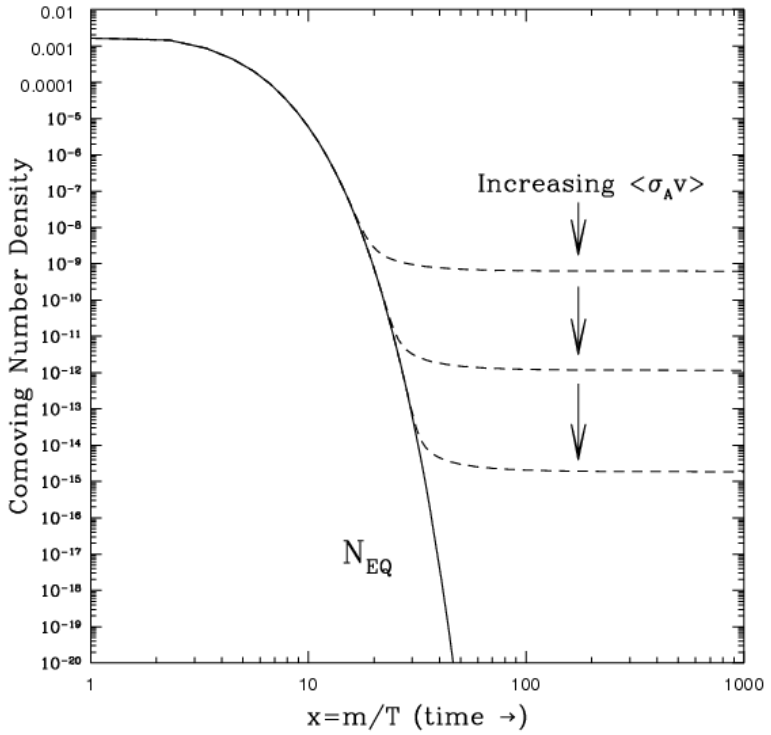

Figure 2.2 A diagram for the thermal freeze-out process of stable co-moving particle densities as the universe expands. The solid line, labelled as N_{EQ}, is the dark matter density that remains in thermal equilibrium as the universe expands. The dashed lines represent the freeze-out dark matter density with varying annihilation rate of $\langle \sigma v \rangle$. To describe the evolution of the Universe based on temperature rather than time, the x-axis variable is defined as the ratio of the particle's mass to the temperature of the Universe. The y-axis represents the co-moving number density of dark matter, which accounts for the number of dark matter particles within a volume that expands along with the Universe [7–9].

Time: 1 s - 3 minutes after the Big Bang

A lot has happened in a very short time after the Big Bang, truly a time for interesting physics. Shortly after neutrinos decoupled, the Universe's temperature dropped below the electron mass, sparking the process of electron-positron annihilation. The energy density and entropy of this annihilation were transferred only to the photons and not the neutrinos. This 'heated' the photons (although not significantly), which can explain why the temperature of the photons is slightly greater than the background temperature of the neutrinos today.

Big Bang Nucleosynthesis

Around 0.1 MeV, the only baryons that existed during this time were free protons and neutrons. Hence, the ratio of neutrons to protons is critical to the outcome of Big Bang Nucleosynthesis (BBN). Around 3 min after the Big Bang, around 100 keV, the Universe cooled below the binding energies of typical nuclei and allowed the formation of light elements. The first nuclei to form were deuterium. The formation of deuterium continued while protons and neutrons were plentiful. Once enough deuterium was available it initiated the production of Helium. This epoch in the Universe provides valuable insight into the formation of hydrogen, helium and lithium and is better understood by the ratio of helium to hydrogen.

Skipping forward to about $50 - 60$ kyr after the Big Bang, at this time, the density of matter increased to more than the density of radiation, giving rise to the matter-radiation equality. The point of matter-radiation equality marks a significant transition between two primary eras in the history of the Universe: one characterized by radiation domination and the other by matter domination [61, 62].

Time: $\sim$ 380 kyr after the Big Bang

Recombination

The early stages of the Universe were extremely hot, which kept the Universe ionized and kept photons tightly coupled to ions. The electrons and ions could recombine as the Universe cooled to form neutral hydrogen freeing the photons. As the number of electrons dropped, the mean free path of photons increased and the Universe became transparent. These photons, as though emitted from a surface at a redshift $z \sim 1100$ corresponding to time $\sim$ 300 kyr after the Big Bang, are now observed as a part of the cosmic microwave background (CMB). This period is called recombination, even though this is when electrons and Hydrogen ions combined for the first time. Electron transitions in hydrogen and helium atoms govern the physics during this time along with their interactions with the background photon field via Thomson scattering. The rate of Thomson scattering is given by $\Gamma = n_e c \sigma_T$ where $\sigma_T = 6.7 \times 10^{-25}\,\mathrm{cm}^2$ is the Thomson cross-section and n_e is the number density of electrons.

During recombination, the assumption of equilibrium conditions allows using a Maxwell-Boltzmann distribution for baryons and Bose-Einstein distribution for photons

to obtain the ionization fraction and equilibrium quantities for various particles. However, as the interaction rate depends on the number density of free electrons and protons, the rate of photon scattering due to electrons goes down when more neutral hydrogen is formed. Hence, eventually, the interaction freezes out. This event of Thomson scattering freeze-out is known as the surface of last scattering or decoupling of photons from baryons. Consequently, the photons start to stream freely through the Universe towards the present time and are detected in the form of the CMB signal. The next chapter will go through the physics and role of the CMB in understanding the evolution of the Universe [61, 62].

Time: $> 100\,\mathrm{Myr}$ since the Big Bang

After the Universe became neutral at recombination, it turned transparent because the photons did not have enough energy to knock out trapped electrons or any free ions to interact with. It was not until gravitational collapse due to dark matter that created the first stars and quasistellar objects that the surrounding hydrogen gas was reionized. It was at this time that photons were able to interact again and we were able to observe the first stars. This epoch is called the reionization epoch. This brings us to the present time, with the age of the Universe at 13.8 Gyr ($\sim 10^{17}\,\mathrm{s}$) and the current temperature recorded at $\sim 0.24\,\mathrm{MeV}$ [61, 62].

2.2 Composition of the Universe

The ΛCDM model (Lambda-Cold-Dark-Matter) is known as the standard model of cosmology and is a parametrization of the most popular Big Bang cosmology model. It provides an accurate description of the formation of the CMB and its power spectra. In this model, matter and energy have been classified into five main categories; baryonic matter, dark matter, dark energy, neutrinos and photons.

Ordinary Matter and Photons

Baryonic matter was relativistic in the early Universe due to the high temperatures. As the Universe cooled and expanded, the kinetic energies of particles dropped below their rest masses and matter became non-relativistic. However, as photons are observed to be relativistic today, they must have played a different role in the history of the

Universe. On the other hand, neutrinos have a small rest mass compared to ordinary matter and were relativistic for a longer period compared to other matter. The more massive neutrinos have since cooled and become non-relativistic; however, the lightest neutrino could still be relativistic today. Notably, during the recombination era, both photons and neutrinos were relativistic and together are considered as radiation [62].

Dark Matter

In the 1930s, J.H. Oort used the Doppler shifts of stars to study their motion in the Milky Way galaxy. He discovered that their velocities hinted at the presence of a lot more mass in the galaxy than previously predicted. Around this time, Fritz Zwicky arrived at the same conclusion by studying the kinematics of galaxies in clusters, especially in the Coma cluster. He discovered that the galaxies in the cluster only accounted for a small fraction of the cluster's mass while the rest was non-luminous [45].

Building on this, in the 1970s, Vera Rubin and her team studied the rotational velocities of isolated galaxies by analyzing observed spectral lines and their Doppler shifts [64]. The motion of celestial bodies in galaxies was assumed to be similar to the movement of planets in our solar system. Newton's law states that the rotational speed of an object in a cluster is connected to its distance from the centre as

$$v(r) = \sqrt{G\frac{m(r)}{r}}, \tag{2.5}$$

where the object is at a distance r from the centre with a velocity $v(r)$, G is the gravitational constant, and $m(r)$ is the total mass inside the volume with a radius of r. As $v(r) \propto \frac{1}{\sqrt{r}}$, it indicates the rate at which the velocity of objects further away from the centre should decrease. This is named 'Keplerian' behaviour [47].

However, Rubin discovered that the rotation curves for velocities of stars continued to increase with distance from the galactic centre up to a limit, and curves were 'flat'. She postulated that extra non-luminous mass further away from the galactic centre must contribute to the velocities. As this was not visible or detectable matter, this has been termed 'dark matter'. Since then, the existence of dark matter has been confirmed by many more complementary astrophysical observations [65].

The ΛCDM model includes cold dark matter as a gravitationally active component. It plays an essential role in the large-scale structure of the Universe, and the formation of galaxies and galaxy clusters. However, its microscopic nature is still out of scientific reach [47, 48].

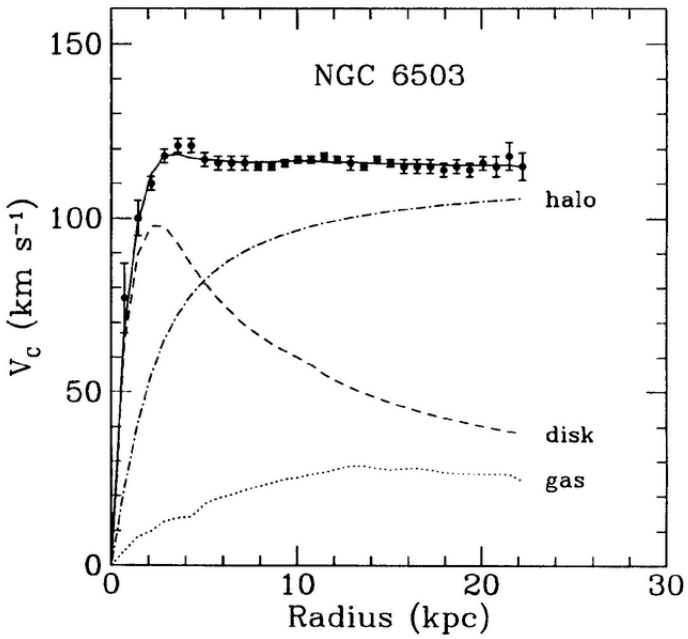

Figure 2.3 Rotational Curve of NGC 6503. The data represents measured circular rotation velocities as a function of distance from the center of the galaxy. Interestingly, adding a dark matter halo followed the observed curve better, (halo+disk) [10].

Dark Energy

In the early 1910s, Vesto Slipher used spectroscopy to investigate the rotational behaviour of galaxies and discovered that the spectral lines of distant galaxies were redshifted. This laid the foundation for the notion that the Universe was expanding. The redshift in the spectrum of an observed galaxy can be defined as

$$z = \frac{\lambda_{\text{earth}} - \lambda_{\text{galaxy}}}{\lambda_{\text{galaxy}}}, \tag{2.6}$$

where λ_{galaxy} is the wavelength of a photon originating at a galaxy and λ_{earth} is its wavelength observed at Earth [26].

Following this work, in 1929, Edwin Hubble discovered a relationship between the recessional velocities of galaxies and distances to them. Named the Hubble law, this

relationship between D, the distance to the galaxy and v, the recessional velocity is mathematically written as

$$v = H_0 D, \tag{2.7}$$

with the Hubble rate, H, measured at $t = 0$, present time. The amount of matter accounted for at the time of this discovery was insufficient to explain the expansion rate. In addition, observations of standard candles, Type Ia supernovae, have recently shown that the expansion is accelerating. This has sparked the inception of a new kind of energy, dark energy, to account for the acceleration making up almost 70% of the Universe [66].

2.3 Summary

In this chapter, we have presented the key events in the history of the Universe that have shaped its evolution and led to quantities measured today. The following are highlights of this chapter

- Characteristics of the Universe after the big bang and its evolution from hot plasma, through to dark matter freeze out and the formation of large scale structure.
- Introduction to the epoch of recombination, studied using the cosmic microwave background - whose data will be usedfor studying the DDM model in this work.
- Composition of the Universe classified into ordinary matter, dark matter and dark energy.

Chapter 3

Parameters of Cosmology

3.1 The ΛCDM Model

The Universe on large scales seems simpler in structure than on smaller scales. The matter distribution is highly irregular on more minor scales, but a large-scale view shows that matter is distributed more homogeneously. Cosmological probes have shown that at sufficiently large distances, the galaxy distribution appears to be homogenous. Additionally, temperature measurements of the cosmic microwave background provide evidence that the Universe is isotropic on the largest scales. This is known as the cosmological principle. Based on this principle and special relativity, cosmologists define a frame at rest with respect to the expanding Universe, called the fundamental observer's frame. Even though the fundamental observers move relative to each other, they are assumed to have no motion with respect to the overall Universe. They will make the exact same measurements for quantities comoving with the expansion of the Universe [67].

Friedmann Equations

The homogeneity and isotropy of the Universe describe the spatial geometry of the Universe. Given these properties, the general line element ds is defined by the Friedmann-Lemaitre-Robertson-Walker (FLRW) metric in polar coordinates in three dimensions (r, θ, ϕ), centered at the observer,

$$ds^2 = dt^2 - a^2(t)\Big(\frac{dr^2}{1-kr^2} + r^2 d\theta^2 + r^2 \sin^2\theta d\phi\Big). \tag{3.1}$$

Here, $a(t)$ is a scale factor that describes the evolution of the Universe and is dependent on time t. The k parameter is a curvature constant that characterizes the spatial geometry of the Universe, with a value of $+1$ for a closed Universe, 0 for a flat Universe and -1 for an open Universe. The evolution of the scale factor with cosmic time is dependent on the energy density in the Universe. Different forms of energy dominated at different periods during the expansion of the Universe. The early Universe was radiation dominated with $a \propto t^{1/2}$, which later turned into a matter-dominated Universe with $a \propto t^{2/3}$ [61–63].

Using this metric and Einstein's general relativity, Friedmann, in 1922, derived mathematical equations defining the equations of motion of the Universe. These equations are now known as the Friedmann equations and are as follows.

$$\begin{aligned} \dot{H}(t) + H(t)^2 &= -\frac{4\pi G}{3}\left(\rho + \frac{3p}{c^2}\right) + \frac{\Lambda c^2}{3}, \\ H(t)^2 &= \frac{8\pi G\rho}{3} - \frac{kc^2}{a^2} + \frac{\Lambda c^2}{3}. \end{aligned} \tag{3.2}$$

Here, H is the Hubble parameter defined as the rate of expansion of the Universe. It can be written in terms of the scale factor $H(t) = \dot{a}(t)/a(t)$. At $t = t_0$, today, the Hubble parameter is $H(t_0) \equiv H_0$, which is the constant used in the Hubble-Lemaitre law as in Eq. (2.7). Often in the literature, the Hubble parameter is written as $H_0 = 100h\text{km s}^{-1}\text{ Mpc}^{-1}$, with h as the dimensionless Hubble constant. The quantity ρ is the energy density. Λ is a cosmological constant associated with dark energy. When considering the global history of the Universe, the Λ term can be thought of as providing an effective acceleration for the expansion.

The Friedmann equation provides an expression for the critical density of the Universe, defined as the matter density required for a spatially flat Universe. By taking $k = 0$ for a spatially flat Universe and $\Lambda = 0$, we get simplified versions of the equations,

$$\rho_{crit} = \frac{3H_0^2}{8\pi G}, \tag{3.3}$$

and the current Hubble constant H_0 at $t = t_0$,

$$H_0^2 = \frac{8\pi G\rho_{crit}}{3}. \tag{3.4}$$

The critical density is further used to define dimensionless density parameters for every component of the ΛCDM model, such as dark energy, baryonic matter, radiation and cold dark matter ($i = \Lambda, b, \gamma, \mathrm{CDM}$) [62]

$$\Omega_i(t) = \frac{\rho_i(t)}{\rho_c}. \tag{3.5}$$

These density parameters are independent of cosmological models and give the proportions of each of the Universe's constituents with respect to the critical density today. A dimensionless quantity, Ω_{tot}, parametrizes the overall geometry and is given by the total energy today at t_0 divided by the critical density required for a flat Universe [62, 63, 68],

$$\Omega_{tot} = \frac{\Sigma_i \rho_i(t_0)}{\rho_c}. \tag{3.6}$$

Assuming a flat Universe, the densities of each component today are expected to add up to 1

$$\Omega_b + \Omega_{cdm} + \Omega_\gamma + \Omega_\Lambda = 1. \tag{3.7}$$

However, for all values of $k \neq 0$, it is necessary to consider the total curvature energy density. This can be corrected for by adding an effective curvature energy density to the equation [62, 63]

$$\Omega_b + \Omega_{cdm} + \Omega_\gamma + \Omega_\Lambda = 1 - \Omega_k \tag{3.8}$$

where,

$$\Omega_k = -\frac{kc^2}{H_0^2} \tag{3.9}$$

Relationship between redshift and scale factor

Almost all of the information about the Universe arrives to us in some form of light - photons. To better study the evolution of the Universe, it is essential to understand the relationship between redshift (z) and the scale factor $a(t)$. Redshift z is defined as the change in wavelength of photons between them being emitted and detected due to the expansion of the Universe.

The redshift-scale factor relationship is given as

$$1 + z = \frac{\lambda_0}{\lambda_1} = \frac{a(t_0)}{a(t_1)}. \tag{3.10}$$

The quantities λ_0 and λ_1 are the wavelengths of light being detected at t_0 and emitted at t_1 respectively. It is important to note that redshift is model-independent, allowing comparisons between various models and quantities. Additionally, redshift is often used in the literature instead of cosmic time, which depends on the constituent quantities of a model [63].

Studying the anisotropies in the Cosmic Microwave Background (CMB) and the distribution of matter at a large scale is the most significant method to understand the evolution of structure and the formation of the Universe within the context of ΛCDM. The following section provides an overview of CMB observables and anisotropies.

3.2 The Cosmic Microwave Background

The period of free streaming photons after the recombination epoch is geometrically constrained in a sphere of last scattering. This sphere has Earth at the centre, and photons from the surface of this sphere travel through the Universe directly to us. Due to the expansion of the Universe, they are observed to be in the microwave region of the electromagnetic spectrum with a current blackbody radiation temperature of $T = 2.7\text{K}$ in all directions. The CMB contains small fluctuations in temperature in the form of anisotropies. The fluctuations in the temperature are affected by the motion of Earth through the photon background. After subtracting the dipole correlation due to this effect, the remaining variations occur at the level of 1 part in 10^5. This suggests that the scattering surface was causally connected at some earlier time. An explanation for this is the period of rapid inflation of the Universe that could have only been driven by a cosmological constant and not matter [69]. Hence, the study of the CMB can provide a powerful way of studying the parameters describing the Universe's evolution.

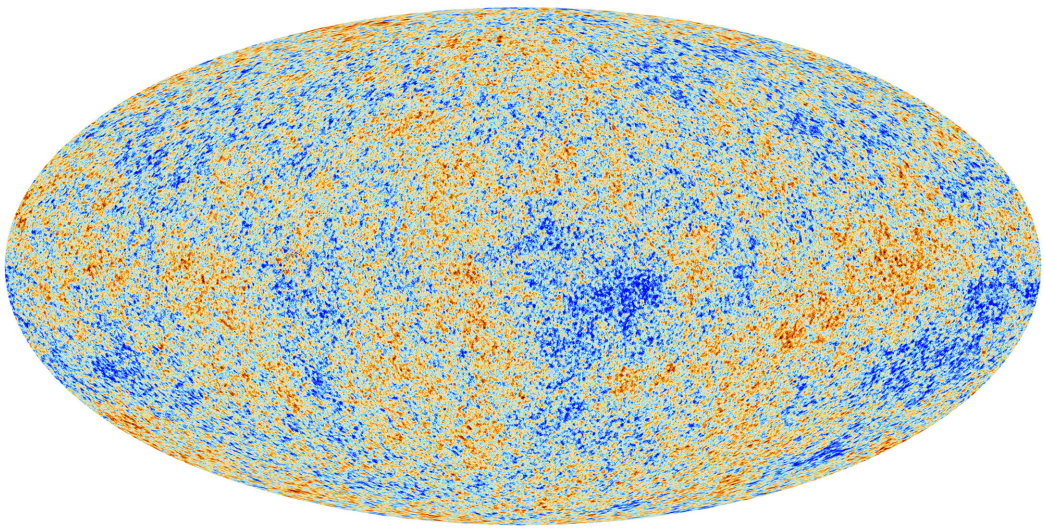

Figure 3.1 Planck image of the Cosmic Microwave Background, a snapshot of the oldest light when the Universe was $\sim 380,000$ years old. It shows tiny temperature fluctuations corresponding to regions of slightly varying densities. [11]

3.2.1 Temperature Anisotropies

The anisotropy power spectrum [2] of the CMB pertains to the spatial scale of temperature variations observed in the CMB over the entire celestial sphere. The temperature anisotropies present in the CMB result from density fluctuations that emerged after the inflationary expansion era, and are characterized by peaks and troughs that are dependent on the Universe's energy content and initial conditions before and after recombination. Despite being minuscule, these fluctuations possess unique features. One of the fundamental observations of the CMB is its intensity concerning frequency and directional variations across the sky, $\hat{\boldsymbol{n}}$.

Quantitative Description

In this section, we will provide a mathematical description for the power spectrum. Any function on the surface of a sphere, denoted by $T(\theta, \phi)$, can be written as a summation of complex functions on the sphere with well-defined wavelengths, the spherical harmonics $Y_{lm}(\theta, \phi)$.

$$T(\theta, \phi) = \sum_{lm} a_{lm} Y_{lm}(\theta, \phi) \tag{3.11}$$

Here, the l value represents the number of spatial oscillations in the θ direction in spherical coordinates and m is the number of spatial oscillations in the ϕ direction. The spherical harmonics of the lowest l values are named, monopole, dipole, quadrapole and octupole for $l = 0, 1, 2, 3$. The quantity a_{lm} is the angular momentum quantum number. Cosmological models are not capable of predicting the exact temperature or value of a specific a_{lm} in a given direction. Instead, these models make predictions about statistical properties, such as the average or mean value and the variance of the a_{lm}. The variance is given as

$$C_l \equiv \langle a_{alm} a^*_{lm} \rangle \tag{3.12}$$

[2] The term spectrum is defined as the distribution of photon intensity (number of photons) as a function of energy (wavelength or frequency).

The power spectrum, denoted by C_l, represents the variance as a function of l. In the context of plotting cosmic microwave background (CMB) data, it is common to use the form $D \equiv l(l+1)C_l(2\pi)$.

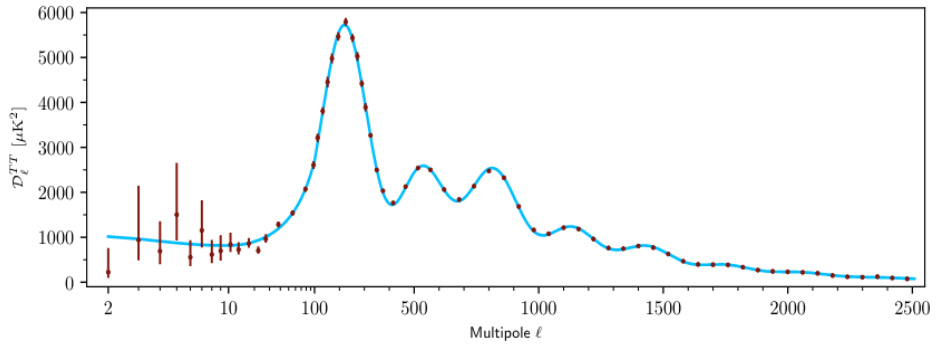

[h!]

Figure 3.2 Planck 2018 TT plot. The blue line depicts the best-fit curve from Planck 2018 to the ΛCDM data, with multipole l on the x-axis and amplitude in units of microKelvin on the y-axis [12].

The first peak in the Fig. 3.2 arises at $l \approx 250$, which corresponds to an angle a little less than 1° on the sky. The position and magnitude of the first peak in the CMB power spectrum offer crucial insights into the composition and geometry of the universe. Specifically, the position of the first peak corresponds to the curvature of space-time; a higher peak suggests a universe with a positive curvature, while a lower peak suggests a negative curvature. The height of the peak is indicative of the density of matter and radiation in the universe, with a taller peak indicating a higher density [9].

The characteristic peaks and troughs in Fig. 3.2 arise due to the interactions of photons and baryons trapped in gravitational potential wells formed due to cold dark matter. The baryon compression results in energy exchange via photons, resulting in oscillatory patterns that are appropriately named acoustic peaks. This oscillatory behaviour, the compression and rarefactions of baryons, results in photons being blue or red-shifted, depending on whether photons fall into wells and heat up (blue) or cool down (red). Hence, this gives rise to temperature fluctuations around the mean temperature T_0. Due to this, as photons are expelled from the wells, they have some non-zero net energy, which contributes to the overall anisotropy. This is called the Sachs-Wolfe effect. In addition, photons also undergo the Doppler effect due to the presence of moving matter around the recombination epoch [70].

The amplitudes, positions (l values), and shapes of the peaks present in the CMB power spectrum provide valuable information about various parameters of our universe,

including baryon density, dark matter density, dark energy density, curvature, and more. It's important to note that a single parameter may impact multiple peaks, while the features of a given peak can be influenced by several parameters. For instance, curvature affects the position of all peaks, while different baryon densities alter the oscillation frequency (slower for more mass) for all standing waves, changing the value of l for each peak, including the first, albeit slightly [71].

The characteristic peaks and troughs in Fig. 3.2 arise due to the interactions of photons and baryons trapped in gravitational potential wells formed due to cold dark matter. The baryon compression results in energy exchange via photons, resulting in oscillatory patterns that are appropriately named acoustic peaks. This oscillatory behaviour, the compression and rarefactions of baryons, results in photons being blue or red-shifted, depending on whether photons fall into wells and heat up (blue) or cool down (red). Hence, this gives rise to temperature fluctuations around the mean temperature T_0. Due to this, as photons are expelled from the wells, they have some non-zero net energy, which contributes to the overall anisotropy. This is called the Sachs-Wolfe effect. In addition, photons also undergo the Doppler effect due to the presence of moving matter around the recombination epoch [70].

3.2.2 Polarisation Anisotropies

Besides temperature variations, the CMB radiation also displays polarisation patterns, offering more understanding into the early universe. The polarisation of the CMB can be categorized into two components: E-mode and B-mode polarisation. The E-mode polarisation is generated by density fluctuations in the early universe, resulting in polarisation patterns with a quadrupolar structure. These patterns resemble those found in the temperature anisotropy maps of the CMB. On the other hand, B-mode polarisation originates from vector and tensor perturbations in the early universe, such as gravitational waves produced during inflation. These produce polarisation patterns, which are not yet detected and tested by standard cosmological models. The E-mode polarisation spectrum shows peaks and troughs that reveal information about the density and curvature of the universe. The B-mode polarisation, however, is much weaker than the E-mode and requires highly sensitive instruments for detection [70, 72].

The radiation in the CMB is polarized at a 10% level due to the Thomson scattering of photons off the surface of last scattering [70]. The Thomson scattering depends on the

polarisation and the differential cross-section for this process is given by

$$\frac{d\sigma_T}{d\Omega} \propto \frac{3}{8\pi}|\boldsymbol{E}' \cdot \boldsymbol{E}|. \tag{3.13}$$

Here, the $\boldsymbol{E}$ and $\boldsymbol{E}'$ are for incident and scattered photons respectively [73]. However, along with its strength, polarisation also has an orientation(ϕ) relative to the strength of two linear polarisation states. The Thomson scattering dictates how the temperature of photons interacting with electrons affects the polarisation of the scattered photons. Similar to the temperature anisotropy, the polarisation of the CMB can be plotted as a function of angular scale.

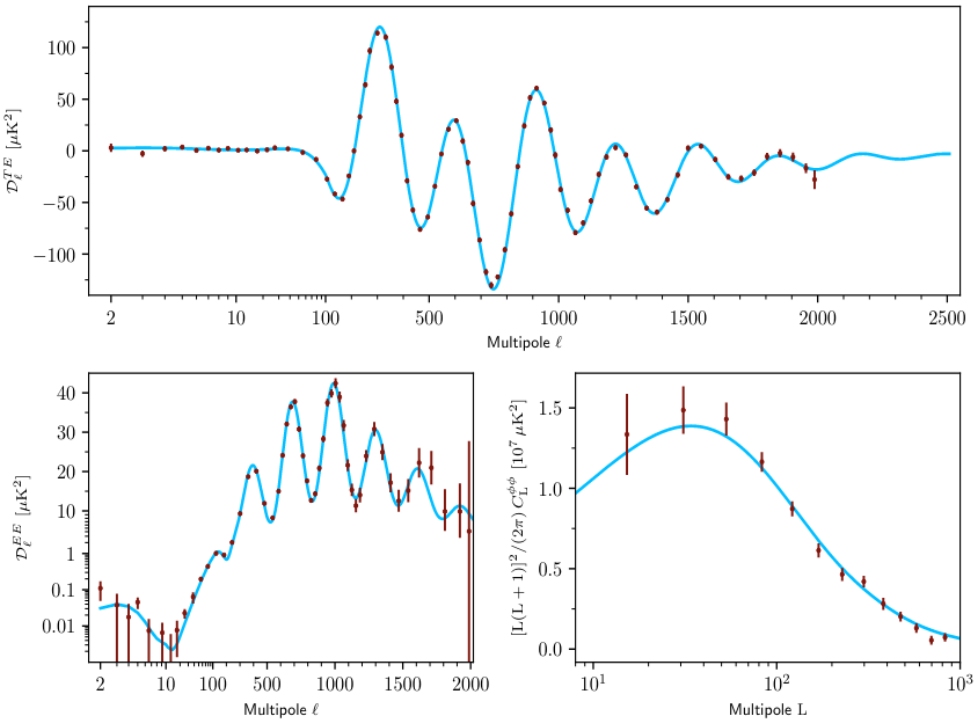

Figure 3.3 Planck 2018 TE (top), EE (bottom left) and $\phi\phi$ (bottom right) plot. The blue line depicts the best-fit curve for Planck 2018 to the ΛCDM data, with multipole l on the x-axis and amplitude in units of microKelvin on the y-axis [12].

Sachs-Wolfe Effect

The Sachs-Wolfe effect is aptly named after R.K. Sachs and A.M. Wolfe, who used the linear matter power spectrum to study the redshift of CMB photons due to gravitational potentials. This effect can be divided into two mechanisms, the integrated Sachs-Wolfe (ISW) effect and the non-integrated Sachs-Wolfe (NISW) effect. The NISW effect is the source of primary anisotropies at larger scales - corresponding to lower multipoles. However, the ISW provides secondary anisotropies to the CMB that relate to the time between today and recombination (surface of last scattering). These depend on the expansion of the Universe when it is not matter-dominated. The presence of relativistic particles in the early Universe (early-ISW) and dark energy dominance in the late Universe (late-ISW) contribute to the ISW effect. Hence, any changes due to dark matter decay can affect the early and/or late ISW effect and although not directly, are expected to pop up in the angular-temperature power spectra of the CMB [74].

3.2.3 Sources of CMB effects

The recombination epoch is essential to understanding the CMB. For this work, it is necessary to understand the effects of exotic energy injection in the early Universe. The main impact on the CMB from any energy injection can be seen due to the changes in the free electron fraction. An important quantity in the reionization period is the free electron fraction given by the equation

$$x_e = \frac{n_e}{n_p(z) + n_H(z)}. \tag{3.14}$$

Here the fraction depends on the number density of electrons n_e, protons n_p and atomic hydrogen n_H. Changes to the free electron fraction reflect in the CMB through the Thomson optical depth and the visibility function $g(z)$. The visibility function is a measure of the probability that a photon was scattered in some redshift interval $[z, z+dz]$:

$$g(z) = \exp\left(- \tau(z)\frac{d\tau}{dz}\right) = \frac{\sigma_T n_e(z)}{(1+z)H(z)}. \tag{3.15}$$

The function $g(z)$ gives the probability distribution for the photon scattering and is dependent on the number density of electrons. Here, $\tau(z)$ is the optical depth at conformal time (related to z) and describes the probability of photon scattering occuring between

that conformal time and the present. Any changes in photon energies or the number of photons around recombination will affect the scattering events, thus affecting the number density of electrons and the CMB anisotropy. A notable effect of rescattering photons is the suppression of CMB peaks by $e^{-\tau}$, as randomized scattering reduces temperature differences in the CMB. The primary effect of the decay model discussed in this work is to change the amount of radiation present around recombination and study its effects [75].

3.3 The ΛCDM Parameters

The Planck data provides six parameters inferred from the CMB for the base ΛCDM model with the help of the Friedmann equations. Their latest values from the Planck 2018 measurements are used to obtain results in this work and are listed in Table 3.1.

Names	Parameters	Values
Dark Matter density	$\Omega_c h^2$	0.120 ± 0.001
Baryon density	$\Omega_b h^2$	0.0224 ± 0.0001
Scalar spectral index	n_s	0.965 ± 0.004
Optical depth	τ_{reio}	0.054 ± 0.007
Hubble constant ($\mathrm{kms^{-1}Mpc^{-1}}$)	H_0	67.4 ± 0.5
Matter fluctuation amplitude	σ_8	0.811 ± 0.006
	S_8	0.831 ± 0.013

Table 3.1 Most recent Planck 2018 values for ΛCDM parameters [12]

The parameters in the aforementioned table will be kept fixed at these values throughout this work.

3.4 Summary

This chapter introduced the parameters defined to measure and study observables of the Universe. The important takeaways from this chapter are,

- Introduction to the ΛCDM model and the density parameters defined for the different contents of the Universe.
- Brief introduction to the Friedmann equations and the Hubble parameter and its relation to the expansion of the Universe.
- The cosmic microwave background (CMB), its observables and power spectrum.
- Contributions to the CMB power spectra due to any energy injection phenomena.
- Most recent values for ΛCDM parameters published by Planck 2018 mission.

Chapter 4

Modelling a Two-step Dark Matter Decay

The aim of this thesis is to expand on the existing literature on decaying dark matter by introducing a two-step decay model. We continue building on the achievements of Ref. [32], and propose a complex decay scenario, incorporating models from Ref. [25,76,77]. Complementary to our model, we present a new version of the Boltzmann code CLASS produced by merging two of its publicly available versions; one that handles the first decay WIMP $\rightarrow$ SWIMP $+ \gamma$, and the second that handles CDM $\rightarrow$ WDM $+ \gamma$ decay.

4.1 CLASS: Boltzmann Code

Cosmologists have become interested in fitting cosmological data and probing extensions of the standard model. As a result, Boltzmann codes such as CMBFAST [78] and CAMB [79] have gained popularity. For the work we present in this thesis, we use another Boltzmann code - CLASS [31], which computes the CMB power spectra for a given set of cosmological parameters by solving the Boltzmann equations. It uses different C modules built within, namely `background`, `thermodynamics`, `perturbations`, `bessel`, `transfer`, `primordial` and `spectra`, to accomplish the computation. Each module handles the various steps necessary for calculating cosmological histories and the resulting power spectra.

For our model, we focus on four important CLASS modules, which are briefly discussed below, in order of code execution.

- `input.c`: The input module reads and allocates the appropriate parameters supplied in the input parameter file, with the suffix '.ini'. The code takes in two types of input parameters; precision parameters and cosmological parameters. All these parameters play a different role in the computation of power spectra such as in the background or thermodynamics modules and are defined under the corresponding structures.

- `background.c`: After the allocation of parameters, the code calls the background module, which contains the Friedmann equations and governs the background evolution of the Universe. When initialized, it integrates the background equations and stores the background quantities as a function of conformal time [3] (τ) in an interpolation table. In addition, it provides functions that allow other modules in the code to evaluate background quantities at a given value of conformal time or find the relationship between redshift and conformal time.

- `thermodynamics.c`: The thermodynamics module calculates the thermodynamical evolution with the help of additional recombination modules such as Recfast [80] or Hyrec [81]. It calculates thermodynamic quantities as a function of redshift z and stores them in an interpolation table. It handles quantities including, but not limited to, recombination time, reionization time and optical depth, and sound horizon at recombination.

  – Sound horizon: In the early universe, photons and baryons formed a plasma that could be treated as a single fluid. As baryons fell into gravitational potential wells, they became compressed and heated up the plasma, which in turn increased the outward radiation pressure from the photons. This process continued until the radiation pressure halted the compression and caused the exapnsion and cooling of the plasma, in turn producing less radiation pressure. The decreased radiation pressure allowed gravity to dominate again, leading to another compression phase. The competition between gravity and radiation pressure set up longitudinal oscillations in the photon-baryon fluid, known as acoustic oscillations. When matter and radiation decoupled at recombination, the pattern of these oscillations became frozen into the CMB. The evidence of these sound waves leading to regions of higher and lower density can be observed in the CMB anisotropies. The sound horizon, r_s, represents the distance that

[3] Conformal time can be defined as the time required for a photon to travel from our location to the farthest observable distance, assuming that the expansion of the universe had stopped [62].

sound waves could have traveled before recombination and is a fixed physical scale at the surface of last scattering [61, 62, 82].

In the following sections, we discuss the modifications made to this module to produce our version of the code.

– Recombination : Thermodynamical quantities during recombination are sampled using recombination codes such as Recfast [80] and Hyrec [81]. Both of these codes handle the physical effects on the free electron fraction and the hydrogen-helium recombination ratios.

- After getting information from the rest of the modules such as `primordial.c` and `transfer.c`, the `spectra.c` module computes the observable CMB power spectra and stores them in its structure `spectra`. Additionally, if lensing is specified in the input file, which is not required for this project, the `lensing.c` module computes the lensing CMB power spectra. At the end, the `output.c` module writes output in various files including the power spectra values.

4.2 Modelling the WIMP decay

Recall that in our proposed decay model, the first step involves the decay of a WIMP into a SWIMP and one or more massless Standard Model particles represented by the symbol S. In our scenario, S represents a photon and will be denoted as γ henceforth. The following section focuses on the phenomenology of this decay and the modifications made to ExoCLASS [83]. Since the SWIMP is practically invisible, detecting evidence of γ production in the early universe is crucial for studying the effects of the decay.

The energy injection from this decay is expected to affect the cosmological history of the Universe. Recall that WIMPs are popular dark matter candidates because their relic density agrees with the dark matter density observed today. Furthermore, due to their extremely weakly interacting nature, SWIMPs also preserve the WIMP relic density, allowing WIMPs to decouple in the early Universe and form the overall dark matter density $\Omega_{\text{WIMP}} \sim \Omega_{\text{DM}}$ [84].

The CMB power spectrum shows the imprint of interactions between baryons and radiation before the formation of structures, such as Compton scattering. Hence, any deviation from thermodynamic equilibrium between photons and baryons results in

spectral distortions in the CMB spectra. Therefore, the CMB spectral distortions can be used to comprehensively investigate the impact of dark matter decay on the physics of the early Universe.

However, the process of thermalization strives to re-establish full thermodynamic equilibrium in the early Universe, which can erase potential spectral distortions in the CMB. This effect is particularly efficient at redshifts greater than 10^6, where it can remove any effects of energy injection during that period. Consequently, this process constrains the lifetime of the WIMP and offers a feasible time period for measuring any decay effects [34].

Parameters of the WIMP decay

In our framework, the WIMPs freeze-out in the early Universe and then decay into SWIMPs that form today's dark matter abundance. In the first decay, referenced as the WIMP decay, the SWIMPs inherit the relic density from WIMPs. Assuming every WIMP decay contributes a SWIMP particle and radiation, the SWIMP density can be given as

$$\Omega_{\mathrm{SWIMP}} = \frac{m_{\mathrm{SWIMP}}}{m_{\mathrm{WIMP}}}\Omega_{\mathrm{WIMP}}, \tag{4.1}$$

where m_i are the component masses. Eq. (4.1) implies that for $m_{\mathrm{SWIMP}} \sim m_{\mathrm{WIMP}}$, the SWIMP represents all of the dark matter relic density.

In this decay scenario, WIMP, the effect on the CMB can be characterised by the lifetime of the WIMP and the fraction of energy released. Mathematically it can be expressed with ζ, the total amount of energy released and ϵ_{EM}, the fraction of radiation released as radiation per WIMP decay. In addition, the number density of WIMPs before the decay, N_{WIMP}, is normalised with respect to the background photon density and is related to the total energy released by the following,

$$\zeta = \epsilon_{\mathrm{EM}} N_{\mathrm{WIMP}} \tag{4.2}$$

According to Feng et al., [52], the lifetime, τ, of the WIMP decaying into a SWIMP is considered to be around $10^5\,\mathrm{s} - 10^8\,\mathrm{s}$. The energy of the photon released in the decay

(E_γ) is related to the mass difference between the WIMP and the SWIMP particles, Δm. The equation for E_γ can be determined using relativistic kinematics

$$E_\gamma = \frac{m^2_{\mathrm{WIMP}} - m^2_{\mathrm{SWIMP}}}{2m_{\mathrm{WIMP}}}. \tag{4.3}$$

The fraction of energy transferred to the decay product-photon is equal to the energy injected into the plasma and can be determined using

$$f_{(DM)} = E_\gamma / m_{\mathrm{WIMP}}. \tag{4.4}$$

Changes in the Universe's thermal history significantly affect the expansion rate, H. As a result, the contribution of decaying dark matter energy density to the total energy density will decrease over time. In addition, any released energy will contribute to Compton scattering between CMB photons and free electrons, which may be observable in the CMB spectra.

The CMB has the perfect blackbody temperature for redshifts $z > 10^6$, and due to thermalization, any deviation from the spectrum is exponentially suppressed at higher redshifts. However, at redshifts, $z < 10^6$, the energy injection process supersedes thermalization and recovering thermal equilibrium is no longer possible. Hence, any deviations are imprinted as CMB spectral distortions, which can be observed today. Spectral distortions provide insight into the physics of energy injection processes in the early Universe. If the WIMP decay happens much earlier in the Universe, it may not directly affect the CMB spectrum. Still, the impacts of the first decay can influence to a second decay by imposing constraints on the parameters of the latter.

4.3 ExoCLASS

For the first step, we have used a modified version of CLASS, called ExoCLASS [83]. The main addition of ExoCLASS to CLASS is a module named DarkAges that calculates the effect of exotic electromagnetic (EM) injection on the free electron fraction (x_e) and the CMB spectra. It includes the setup for various scenarios such as dark matter annihilation, dark matter decay and primordial black holes.

The main impact of the exotic energy injection is the effect on the free electron fraction (x_e) evolution, the Thomson optical depth τ_{reio}, and in turn, the visibility function $g(z)$. Accounting for both direct ionization and indirect collisional excitation due to photons, the code suitably calculates the x_e value. It also finds the temperature evolution of the intergalactic medium (IGM), T_m, which feeds back into the x_e calculation. The evolution of T_m and x_e are governed by equations involving the recombination and ionization rates, which are derived in detail in Ref. [83]. As a result, the energy injection processes impact the CMB power spectrum via the Thomson interactions between CMB photons and electrons. Furthermore, the recombination, ionization and heating rates depend on the rate of energy deposited at redshift z and its splitting between the multiple processes of energy dispersion. The energy deposition rate with respect to the rate of energy injection and the fraction of energy split can be written as

$$\left.\frac{dE}{dVdt}\right|_{dep}(z) = f_c(z)\left.\frac{dE}{dVdt}\right|_{inj}. \tag{4.5}$$

Here, the dV is the unit volume of space and dt the unit time.

In ExoCLASS, $f_c(z)$ are defined as the energy deposition functions, which are calculated using transfer functions, T_c. Transfer functions are further defined as the fraction of energies E injected at a redshift z' but deposited at a different redshift z, via given channels c, for a particle such as an electron/positron or a photon. The authors of Ref. [85] show that for a WIMP annihilation scenario, the energy injected around or during recombination is not deposited *on-the-spot*, that is, energy injection and deposition happen at different redshifts. This will be assumed for the decays in this work too. This means that the Boltzman equations require more involved solution techniques and not just stationary approximations. Thus, we use the advanced transfer function calculations in ExoCLASS, assuming that the modified free electron fraction does not back-react onto the energy cascade [83].

In addition to the fundamental ΛCDM model parameters, the decay WIMP $\rightarrow$ SWIMP $+ \gamma$ is parametrized by two free parameters; the rate of decay width Γ (or decay lifetime τ) and the fraction of decaying dark matter. For an arbitrary WIMP decay, the lifetime and the fraction of energy injected by radiation E_γ are considered independent. The implementation of injection history for a DM decay scenario in ExoCLASS is given

as

$$\left.\frac{d^2E}{dVdt}\right|_{\text{inj,decay}} = \Xi\rho_c c^2\Omega_{\text{CDM}}(1+z)^3\Gamma\exp(-\Gamma t). \tag{4.6}$$

The different parameters in the equation are specified in Table 4.1

Parameter	Definition	Notes
Ξ	fraction of decaying dark matter	$\Xi \equiv \rho_{\text{DDM}}/\rho_{\text{CDM}}$
Γ	rate of decay/decay width	$\Gamma^{-1} = \tau$, lifetime in seconds
ρ_c	critical density today	
Ω_{CDM}	fractional DM density today	
z	redshift	

Table 4.1 Parameters for energy injection in a decaying DM scenario, Eq. (4.6)

DarkAges

The DarkAges module of ExoCLASS consists of different python files defined briefly below.

- `common.py` includes all the algorithms necessary for energy deposition calculations.
- `evaporator.py` contains the definitions of functions used in the evaporating black holes scenario.
- `interpolator.py` contains definitions of mathematical classes used to perform logarithmic, linear or N-dimensional interpolations.
- `model.py` is an important module that contains the definition of the model class and its derived classes for different energy injection scenarios, such as the annihilation, decay, accretion and evaporation of primordial black holes. This thesis will mainly focus on the `decay_model` related to decaying dark matter.
- `recipes.py` contains important functions used to calculate the $f(z)$ functions, depending on the energy injection scenario. In addition, it contains functions that read spectra of particles specified as decay products.
- `transfer.py` contains the definition of the transfer class, which stores discretized transfer functions using the kinetic energies of the particles under consideration and the redshifts of energy deposition and injection.

Modifications to ExoCLASS

We made the following modifications to DarkAges of ExoCLASS to handle the WIMP decay.

- To account for the energy of the photon released in the decay, E_γ, we introduced a new input parameter, `photon_energy`, with the units of GeV. We also declared it in the *./bin/DarkAges* file, a script that reads the input parameters in DarkAges and propagates them to appropriate variables in the base CLASS code. The `photon_energy` parameter plays an important role in the `decay_model` function defined under the `model.py` module. It is important to note that the parameter `DM_mass` is the mass of the parent CDM particle.

- In the `recipes.py` module, an important function we were interested in is the `loading_from_specfiles` function that reads files containing tabulated spectra of particles created as decay products. When specifying a decay, the code requires the spectrum of decay product particles either be calculated from first principles or read from a tabulated spectrum given by PPC4MID [86]. To specify a photon as one of the decay products we used the parameter labelled as `dirac_photon`, which was already present in ExoCLASS.

  Originally, if `dirac_photon` is specified as the decay product, it is assumed that a parent particle of mass m decays into two photons, each with energy $m/2$. In the model presented in this thesis, we modified the definition of `dirac_photon` to only release one photon with energy equal to value specified for `photon_energy` in the input file. This value is derived from Eq. (4.3). Next, this function calls the `decay_model` function.

- In `decay_model` function in the `model.py`, after initialization, the spectra of the particles specified in the input file are read and then transferred to the base model-class to calculate the differential equation,

$$\frac{\mathrm{d}^2 N(t,E)}{\mathrm{d}E\mathrm{d}t}, \tag{4.7}$$

  where $d\mathrm{N}/d\mathrm{E}$ is the injected energy spectrum of particles in the decay. After adding the new `photon_energy` parameter, we set the normalization of the energy spectrum of particles to be calculated with respect to the parent CDM particle mass that uses the energy of the photon.

- To prevent issues that occur when all of the parent CDM particles decay into radiation, we used the `decay_fraction` parameter to define the amount of dark matter decay. This value can be found in the mass of the parent particle is fixed, and the energy of the photon is provided, which are related as $f_{DM} = \mathrm{E}_\gamma/\mathrm{m}_{\mathrm{WIMP}}$. If set to 1, it corresponds to all the CDM decaying into radiation, resulting in an unphysical scenario. However, to have the correct abundance of CDM as observed today and not have extreme energy injection change the thermal history significantly, the decay fraction needs to be extremely small, which corresponds to small photon energies.

The amount of energy release and their redshifts are important when investigating the effect of DM decay on the thermal history. The decay width/lifetime and the

photon's energy are currently treated as independent parameters. For the WIMP decay proposed in this thesis, the neutralino (bino) decaying into a gravitino and a photon, the lifetime/decay width of the WIMP is dependent on the decay fraction and the energy of the photon, which will be discussed in detail in the next chapter.

4.4 Modelling the WDM decay

For the second step in our decay scenario, we considered the SWIMP produced in the first decay as the parent particle that further decays into a massive warm, dark matter particle and a massless particle or dark radiation, CDM $\rightarrow$ WDM + DR.

We use the WDM model discussed in Ref. [32] and complement it with results from Ref. [76]. We choose a WDM decay model to leverage the success of Ref. [32], where the authors effectively addressed the S_8 tension. Similar to the first decay, the parameters that characterise the second decay are the decay width/lifetime (Γ/τ) and the fraction of energy transferred to the warm massive daughter particle (ϵ). The decay fraction $f_{\rm DM}$, which represents the portion of dark matter that can decay into warm decay products, is subject to strong constraints in this scenario. Specifically, it must be adjusted to match present-day measurements of the total amount of dark matter and to enable the formation of large-scale structure. So, the maximum amount of CDM that can decay into warm dark matter is limited to 15.

4.4.1 Implementation of WDM in `class_decays`

Before discussing the modifications we made to CLASS for the second decay, we briefly discuss its base NCDM implementation. The definition of NCDM is non-cold dark matter that can be considered massless during the early Universe. Massive neutrinos, sterile neutrinos and warm dark matter are some examples of NCDM species. CLASS uses the formalism defined in Ref. [87], to describe the evolution of NCDM species using massive neutrino equations. By default, it contains a limited version of an ultra-relativistic fluid approximation for NCDM species switched on inside the Hubble radius, especially for warm dark matter particles. In our decay scenario, CDM $\rightarrow$ WDM + DR, the CDM parent particle can be described as a perfect fluid. However, calculating density perturbations for the WDM daughter particle is more complicated. Abellan et al. in Ref. [28] have devised a new fluid approximation in which the WDM is considered a viscous fluid, built on the original implementation in CLASS. We have used the code modified with the new WDM fluid approximation, `class_decays`, to handle the second step in our decay model. We add the first decay to `class_decays` to produce our version of the code.

The authors of Ref. [28] have adopted the Boltzmann formalism from Ref. [88], which discusses the time evolution of the phase-space distribution function (PSD) for the mother and daughter particles in a WDM decay. The authors of Ref. [88] further state that the Boltzmann equation describes the time-evolution of the PSD $f(\boldsymbol{x}, \boldsymbol{q}, \tau)$, where $\boldsymbol{q}$ is the comoving momentum of a particle related to its physical momentum by the scale factor ($\boldsymbol{q} = a\boldsymbol{p}$) and τ is the conformal time. The background evolution of the mother and the daughter particles can then be written in terms of the mean energy density and pressure,[1]

$$\dot{\overline{\rho}}_{\rm wdm} = -3H\overline{\rho}_{\rm dcdm} - a\Gamma\overline{\rho}_{\rm dcdm} \tag{4.8}$$

$$\dot{\overline{\rho}}_{\rm dr} = -4H\overline{\rho}_{\rm dr} - \epsilon a\Gamma\overline{\rho}_{\rm dcdm} \tag{4.9}$$

$$\dot{\overline{\rho}}_{\rm wdm} = -3(1+\omega)H\overline{\rho}_{\rm wdm} + (1-\epsilon)a\Gamma\overline{\rho}_{\rm dcdm} \tag{4.10}$$

Here, the $H = \dot{a}/a$ parameter is the conformal Hubble parameter, $\overline{\rho}$ is the pressure of the labelled dark matter component, and ϵ is the fraction of the mother particle's rest mass energy transferred to the massless daughter. The ω is the WDM equation of state (EoS) that can be written in terms of the mean energy density $\overline{P}_{\rm wdm}$ and pressure $\overline{\rho}_{\rm wdm}$; related as $\omega(\tau) = \overline{P}_{\rm wdm}/\overline{\rho}_{\rm wdm}$. The above equations are evaluated in the `background.c` module of the code, which the authors of Ref. [28] use to derive the new fluid equations for WDM. For a detailed derivation of the new viscous-WDM fluid approximation scheme, refer to Ref. [28].

Parameters of `class_decays`

The authors of Ref. [28] have added the WDM decaying dark matter case on top of the base CLASS module structure. We describe the important parameters defined under the code's WDM-DCDM scenario in the following list.

- The $\Omega^{\rm ini}_{\rm wdm}$ parameter is defined as the density of dark matter decaying into dark radiation and warm dark matter. In the WDM scenario, the value for $\Omega^{\rm ini}_{\rm wdm}$ is provided instead of $\Omega_{\rm cdm}$. When specified as true (non-zero value), it activates the computation of the WDM species in the code. It is also considered in the total energy budget equation in the code.

[1] 'dcdm' stands for decaying cold dark matter and this abbreviation is used throughout CLASS to define the parent decaying dark matter particle.

- The `Gamma_dcdm_wdm` (Γ units of kms^{-1} Mpc^{-1}) and `tau_dcdm_wdm` (τ units of s) are the decay width and lifetime of the decay respectively.

- The `epsilon_dcdm_wdm`(ϵ) parameter is the fractional rest mass energy of the mother particle transferred to the massless daughter particle. Mathematically, it can be written as,

$$\epsilon = \frac{1}{2}\left(1 - \frac{m^2_{\mathrm{wdm}}}{m^2_{\mathrm{dcdm}}}\right). \tag{4.11}$$

  As ϵ is dependent on the ratio of the dark matter particles in the decay and is defined in the input file, the individual masses of the CDM (M_{dcdm}) and WDM particles are not required. Hence, the M_{dcdm} parameter is set to 1 to avoid any technical errors due to a zero value.

- `N_ncdm` and `background_ncdm_distribution` are some of the extra flags required for the code to run the WDM calculations. The authors of Ref. [28] have shown that the system of Boltzmann hierarchy equations for a WDM scenario is similar to the massive neutrino scenario of Ref. [87]. As neutrinos and WDM daughter particles are considered NCDM species, the parameter `N_ncdm` is by default set to 2 to account for both of the species. Following this, the parameter `background_ncdm_distribution` is defined as a list with a length equal to the number of decay products. The values 0 and 1 correspond to the flags for neutrino and WDM species, respectively.

We keep the definition of the WDM parameters unchanged and only make modifications to add the first decay on top of this version of `class_decays` code.

4.5 Code Development

A major part of the work presented in this thesis was based on a new version of the code produced to handle complex decaying dark matter scenarios not limited to cold dark matter species. This section will outline the steps to merge the code handling the first decay, ExoCLASS, with the code running the second decay, class_decays. The production of a new code version was a non-trivial task and required in-depth studying and testing.

- The first step in the process of combining the two codes was to define relevant parameters required for the first decay transferred from ExoCLASS.
  - `Gamma_dcdm_exo` and `tau_dcdm_exo`
  - `photon_energy`
  - `on the spot`
  - `energy_deposition_function` set to 'DarkAges'
  - `DarkAges_mode` set to 'built_in'
  - `energy_repartition_coefficient` set to 'no_factorization'
  - `DM_mass`
  - `injected_particle_spectra`
  - `injected_particle_branching_ratio`

  The changes made were mainly for the `thermodynamics` and `input` modules, and these parameters were declared in the necessary `*.h` files.

- The DarkAges module in ExoCLASS was contained in its directory, which was copied into the modified code directory along with its changes as described in section 4.3.

The input module

- In the input module, we added a `'first_decay'` flag, which is set to 1 in the input-parameter file, would allow the code to read and activate the first decay. And if set to 0, the code would ignore the first decay entirely.
- Then, we added functions that read and assigned values to parameters from the input file, ensuring that the parameters for the first and second decay were defined differently.
- The input module consists of various tests that check if a parameter has appropriate values and has not been declared more than once. Following this, we transferred all the necessary parameter declarations from ExoCLASS. We mainly focused on the decay parts of the code, although the annihilation section was included but not tested rigorously.

The background module

- The major change that we made to the background module, including the `.c & .h` files, was renaming the `Gamma_dcdm` to `Gamma_dcdm_wdm`.

The thermodynamics module

The thermodynamics module was modified to the greatest extent. The `class_decays` code is a newer version of CLASS compared to ExoCLASS. However, the thermodynamics modules in both versions are comparatively similar except for specific energy injection scenarios present in ExoCLASS, which we transferred over to our version of the code. As needed, any new function or parameter names were declared in the corresponding `.h` files.

- ExoCLASS's handling of the DarkAges functions, parameters, DM decay and annihilation was transferred over to the thermodynamics module of `class_decays`. The thermodynamics module in ExoCLASS contained additions of the energy repartition and efficiency functions modified by Vivian Poulin and Patrick Stoecker, which were added to our working thermodynamics file.

- The authors of ExoCLASS modified the recombination code Hyrec. It produced a version that included the energy injection functions and the various differential equations for energy injection and deposition (Eq. (4.5)). Hence, the Hyrec folder was also moved to our current working folder and added to the path.
- Having the ExoCLASS Recfast module within the thermodynamics module was causing technical errors, but replacing it with the newer version did not completely resolve the issues either. Hence, we used HyRec entirely for our analysis.

An important part of merging the code was testing the merged code and checking if the outputs were scientifically reasonable. For this, we defined an input parameter file that is detailed in Appendix.

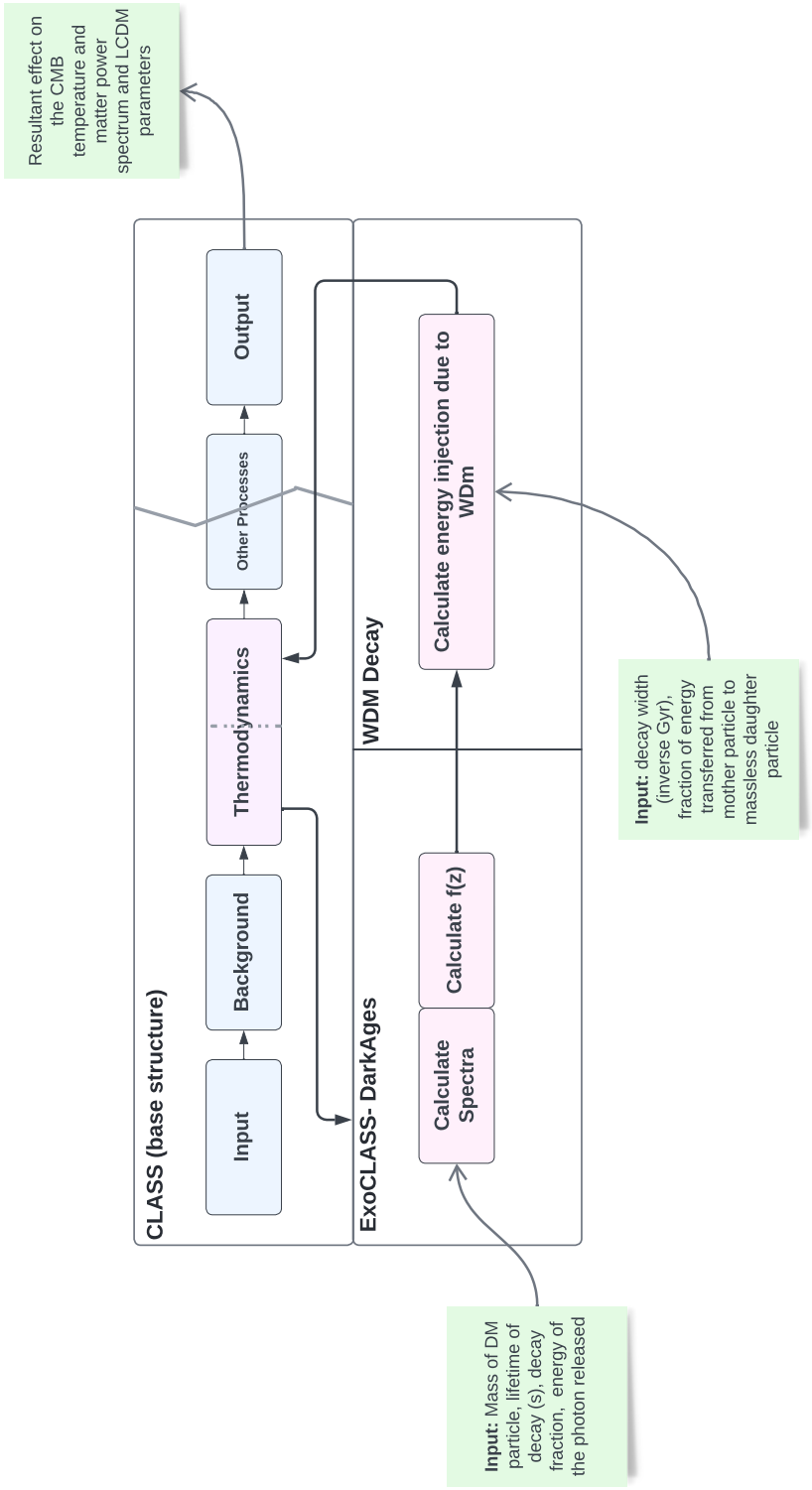

Figure 4.1 Outline of changes made to merge two modified versions of CLASS to handle the two-step decay.

4.6 Code Verification

We reproduced results from the ExoCLASS [83] and `class_decays` [28] publications separately to verify the output of our newly merged code. To check the results for ExoCLASS, we varied the lifetime of the WIMP parent particle and the energies of the photon released in the decay while keeping the second decay deactivated. To verify that the second WDM decay code output the same results as its version before the modifications, we reproduced the results from Ref. [15] and ignored the first decay.

WIMP decay

We consider two sets of parameters for the first decay to generate a set of results. The parameters were: $\{H_0, \omega_{\rm b}, \omega_{\rm cdm}, A_s, n_s, z_{reio}\} + \{\tau_{\rm dec}, E_\gamma\}$. In this scenario, the WIMP mass was fixed to 100 GeV, and the SWIMP mass was varied by small amounts to obtain the Δm values, which provided the values for E_γ. We also varied the lifetime values, $\tau_{\rm dec}$ and compared the output against the base ΛCDM model.

Parameter	Values
ω_b	0.0224
ω_{cdm}	0.12038
z_{reio}	8.24
H_0 (km s^{-1}Mpc^{-1})	67.70
n_s	0.9673
$\ln(10^{10})A_s$	3.052

Table 4.2 Planck 2018 ΛCDM parameters that were fixed for testing code [12].

For the values of $\tau_{\rm dec}, f_{DM}$ and E_γ defined in Table 4.3, the the power spectrum of the CMB temperature was plotted as shown in Fig. 4.2.

E_γ Values (GeV)	τ_{dec} Values (sec)
10^{-2}	10^{19}
10^{-3}	10^{22}
10^{-4}	10^{25}
10^{-5}	10^{31}

Table 4.3 WIMP decaying into a SWIMP and photon decay: decay lifetime (labelled as τ_{dec}) and energy of the photon (E_γ).

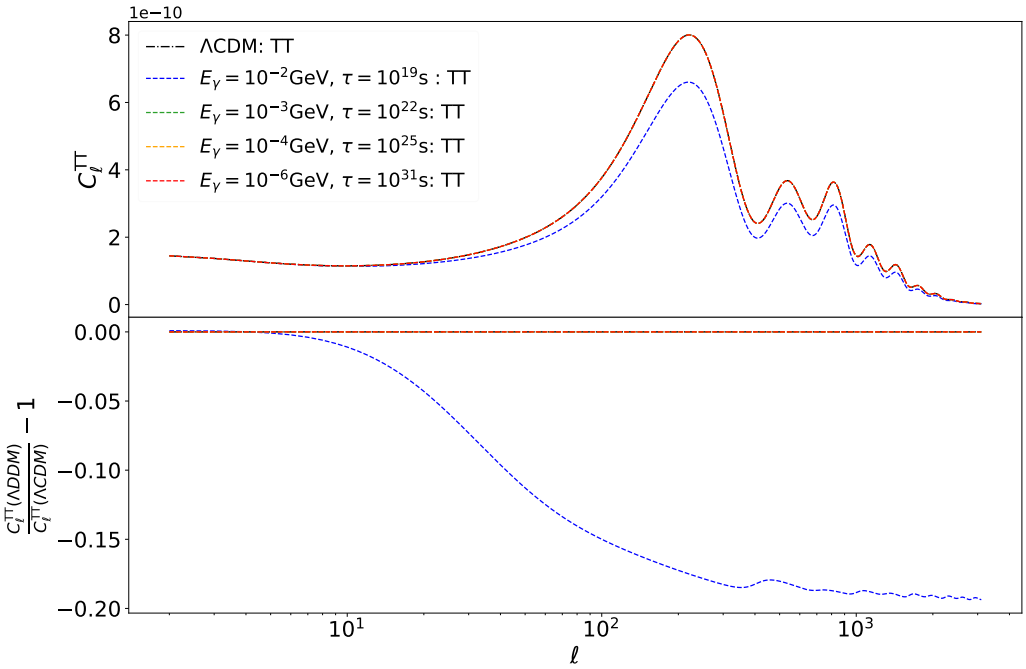

Figure 4.2 WIMP decay to SWIMP and photon for lifetimes $\tau_{dec} > 10^{19}$ s.

The energy injection due to dark matter decay and the spectral distortions depend on the lifetime of the DM particle and its abundance. In addition, the constraints on model parameters also depend on the DM lifetime values. For lifetime values $\tau_{dec} \geq 10^{13}$ s, the CMB anisotropies are heavily constraining, whereas for lifetime values 10^{-1} s $\leq \tau_{dec} \leq 10^{8}$ s, the BBN predictions are the most constraining observations. As stated in Ref. [77], the intermediate lifetime values can be studied using spectral distortions (SDs). Hence, in Fig. 4.2 with $\tau_{dec} > 10^{19}$ s, it can be seen that lifetime increases to more than the age of the Universe ($\sim 10^{17}$ s), the temperature curves for the CMB approach the ΛCDM curves, mimicking a stable dark matter particle scenario. That is, all curves, except the

blue curve corresponding to $\tau_{\rm dec} = 10^{19}$ s, appear overlapped to the black ΛCDM curve, with hardly any significant deviations.

4.7 WDM decay

We reproduced Fig. 5 from Ref. [28] as a test to check if our merged code could output the same result. The parameters we used for this decay were $\{H_0, \omega_{\rm b}, \omega_{\rm cdm}, A_s, n_s, \tau_{reio}\} + \{\Gamma_{\rm wdm}, \epsilon\}$ with the values given in Table 4.4.

Parameter	Values
$\omega_{\rm b}$	0.0224
$\omega_{\rm cdm}$	0.1194
$\tau_{\rm reio}$	0.0582
H_0(km s^{-1}Mpc^{-1})	67.70
n_s	0.9673
$\ln(10^{10})A_s$	3.052
$N_{\rm ur}$	2.0328
$T_{\rm cmb}$	2.7255
$N_{\rm ncdm}$	2
ncdm distribution	0, 1
$M_{\rm ncdm}$	1
$m_{\rm ncdm}$	0.06, 0

Table 4.4 Input parameters and values for analysis.

In addition to the WDM parameters described in section 4.4, the code uses $m_{\rm ncdm} = 0.06$ to find the effective number of neutrinos ($N_{\rm eff}$). The 0.06 value for $m_{\rm ncdm}$, relates to Σm_ν and is constrained to be consistent with the neutrino oscillation experiments. As the mass of the daughter WDM particle is determined by the mass of the parent particle and ϵ parameter, we specified the second value for $m_{\rm ncdm} = m_{\rm wdm}$ as 0. The length of $m_{\rm ncdm}$ depends on the number of daughter particles specified in the decay.

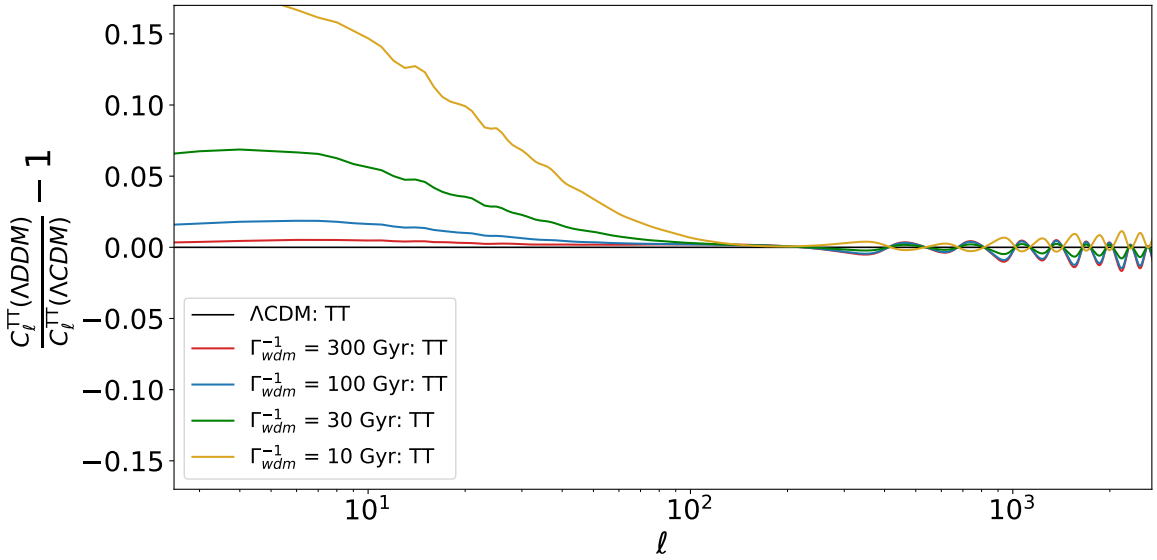

Figure 4.3 Residual plot for the power spectrum of the CMB temperature, $\epsilon = 0.1$ and Γ_{wdm} varied. The TT stands for temperature curves for the CMB power spectrum. The x-axis for Fig. 4.3 and Fig. 4.4 is a logarithmic scale for multipole values, l and the y-axis represents the residuals of C_l's (power) between the decaying dark matter model and ΛCDM model.

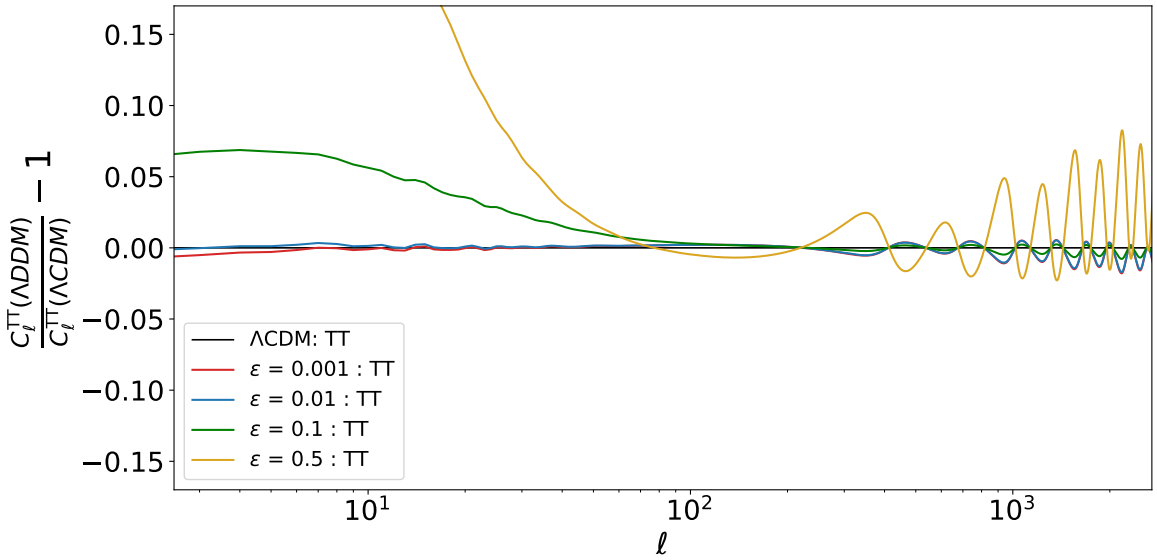

Figure 4.4 Residual plot for the power spectrum of the CMB temperature, $\Gamma_{wdm}^{-1} = 30$ Gyr and ϵ varied.

The residual plots of the CMB power spectrum are depicted in Figure 4.3, with the Planck2018-ΛCDM model [12] data serving as the baseline, indicated by a horizontal line at the C_l residual value of 0.00. The value of $\epsilon = 0.1$ indicates the proportion of total energy gained by the massless daughter particle (photon), with the majority being transferred to the massive decay product, rendering it a warm dark matter particle. As shown in Fig. 4.3, the impact on the temperature CMB power spectrum becomes more noticeable as the lifetime decreases. This is due to the reduction in the matter density ($\Omega_{\rm m}$) caused by the decay, resulting in an earlier onset of the energy-domination era and an increase in Ω_Λ. Consequently, the modified Late Integrated Sachs Wolfe effect manifests as a signature in the low-l TT power spectrum, causing power spectrum curves of the decay model to deviate away from the ΛCDM line in this region.

Figure 4.4 shows the residual plots for a fixed lifetime of $\Gamma^{-1}_{wdm} = 30\,\text{Gyr}$ and varied values of ϵ. When ϵ is smaller, it corresponds to a more significant contribution from WDM, and the increase in Ω_Λ is less pronounced than in the scenario shown in Figure 4.3. As a result, the effect on $\tau_{\rm reio}$ is reduced, and the impact on the low-l parts of the power spectrum is less noticeable in Figure 4.4 than in Figure 4.3. Decays with $\epsilon \leq 0.001$ correspond to non-relativistic decays, as the contribution of the decaying WDM to the matter density is offset by a decrease in the density of the decaying CDM. So the WDM species is almost indistinguishable from the standard CDM.

Conversely, if $\epsilon \simeq 0.5$, the decay is considered relativistic as the WDM decay product acts as a dark radiation component, which can significantly reduce the expansion rate and prevent any matter clustering. However, for values of ϵ ranging from 0.001 to 0.5, the WDM component only partially contributes to the matter-energy density, resulting in an unchanged expansion rate. Hence, as asserted in Ref. [28], any net effect on the CMB power spectrum is similar to the one caused by massive active neutrinos.

According to Ref. [28], solely considering a WDM decay is not sufficient to resolve the two cosmological tensions simultaneously, but only the S_8 tension. To resolve the S_8 tension, the decay should occur with specific values of $\Gamma^{-1}_{wdm} = 55, \text{Gyr}$ and $\epsilon = 0.07$. Recall that the relationship between the S_8 parameter and total matter density Ω_m is $S_8 \equiv \sigma_8\sqrt{\Omega_m/0.3}$. The choice of Γ and ϵ values is based on the fact that the decay into WDM with these parameters leads to a decrease in the amplitude of the matter power spectrum, resulting in a decrease in σ_8 at later times. This decrease in σ_8 leads to a decrease in S_8, resolving the tension, without significantly affecting Ω_m.

The figures obtained using our code are consistent with the findings reported in Ref. [28]. However, the minor fluctuations in the spectrum shown in Fig. 4.3 and Fig. 4.4 are more pronounced in our plots than in the referenced results. These fluctuations may arise during the calculation of the power spectrum due to inconsistent numerical approximations in internal CLASS configurations. It is also possible that our modifications to the thermodynamics module have had some impact on the power spectrum calculation, although this effect is not significant. Despite these issues, the general agreement between our findings and the published results is reassuring and suggests that the resolution of the S_8 tension by the WDM decay model is valid.

4.8 Summary

In this chapter, we provided a detailed account of the Boltzmann code, CLASS [31], and our modifications made to it to handle our DDM model. It includes the following.

- Definitions of the parameters and modules of the base version of CLASS, a modified version by the authors of Ref. [83], ExoCLASS and another modified version accompanying Ref. [28] named `class_decays`.
- Details of our two-step decaying dark matter model and its implementation in a modified version of CLASS.
- Verification of results obtained using our version of CLASS against the base ExoCLASS and `class_decays`.

In this chapter, we describe in detail the technical foundation that was necessary to build and study our decaying dark matter scenario. We are currently working on improving our code to better understand the physics encoded in CLASS, ExoCLASS, `class_decays` and our version in this thesis.

Chapter 5

A Supersymmetric Realization of the Two-step Decay Model

Supersymmetry provides an elegant solution to the hierarchy problem in the standard model by extending its particle spectrum. The extension of the particle spectrum provides plenty of candidates for dark matter. This chapter discusses specific MSSM dark matter particles and their properties that fit the two-step decay scenario we present in this work.

SWIMPs form a popular class of cold dark matter that naturally inherit the desired relic density from the late decays of the WIMPs. However, they are extremely weakly interacting, which limits the ability of direct-indirect experiments to constrain the SWIMP parameter space. Along with temperature and polarization information, the energy spectrum of the CMB provides detailed insight into the thermal history of the Universe at very early times. In the early Universe, any perturbation of the complete thermodynamic equilibrium between photons and baryons leads to spectral distortions in the CMB. So, any additional energy release signatures should be present in the CMB spectrum. This makes cosmological observations an excellent alternative for probing SWIMP dark matter, which will be discussed in detail here.

We base our decaying SWIMP-dark matter model on the framework discussed in Ref. [25]. SWIMPs are produced in the decay of WIMPs but are not detectable in experiments. However, in WIMP decays such as WIMP$\rightarrow$SWIMP+γ, the signatures of the SWIMPs are visible only through observational signals for effects produced in the early Universe by radiation, γ. Hence, the observable consequences only depend on the WIMP's lifetime and the total energy released in the decay. In supersymmetry, the neutralino is one of the thermal-favoured WIMP candidates, which we will focus on in this work.

In this chapter, we extend the literature presented by Ref. [25] and [76] by explicitly studying the neutralino decay into the gravitino. For this decay, any particle candidate that satisfies the conditions for a SWIMP could replace the gravitino, and a similar analysis could be performed.

5.1 Neutralino decay into Gravitino

For the first decay, which is a WIMP decaying into a SWIMP, we take a neutralino as the WIMP and gravitino as the SWIMP decay product. The neutralino, χ_1^0, is a mixture of the neutral bino, wino and higgsino and can be mathematically expressed as

$$\chi_1^0 = U_{\tilde{B}}\tilde{B} + U_{\tilde{W}}\tilde{W}^0 + U_{\tilde{H}_u}\tilde{H}_u^0 + U_{\tilde{H}_d}\tilde{H}_d^0, \tag{5.1}$$

where $\tilde{H}_u^0$ and $\tilde{H}_d^0$ are up and down higgsinos respectively. For the lightest neutralino, we specifically consider a bino-like neutralino, with $U_{\tilde{B}}\tilde{B} \simeq 1$ and $U_{\tilde{W}}\tilde{W}^0 \simeq U_{\tilde{H}_u}\tilde{H}_u^0 \simeq U_{\tilde{H}_d}\tilde{H}_d^0 \simeq 0$. With this neutralino, the decay process looks like $\chi_1^0 \to \tilde{G}\gamma$, with $\tilde{G}$ and γ being the gravitino and the photon respectively. The decay rate for this process is dependent on the masses of the bino and the gravitino, especially on the difference between them (Δm),

$$\Gamma = \frac{\cos^2}{48\pi M_*^2}\frac{m_{\chi_1^0}^5}{m_{\tilde{\mathrm{G}}}^2}\left[1 - \frac{m_{\tilde{\mathrm{G}}}^2}{m_{\chi_1^0}^2}\right]^3\left[1 + 3\frac{m_{\tilde{\mathrm{G}}}^2}{m_{\chi_1^0}^2}\right]. \tag{5.2}$$

As shown in Eq. (5.2) when $m_{\tilde{\mathrm{G}}} \sim m_{\chi_1^0}$, the decay lifetime becomes relatively long. The decay lifetime, (recall that $\tau \propto \Gamma^{-1}$) can be given as

$$\tau = 2.3 \times 10^7 \mathrm{s}\left[\frac{100\mathrm{GeV}}{\Delta m}\right]^3. \tag{5.3}$$

The energy of the SM particle (photon) released in this decay is E_γ. Recall, this energy can be calculated using

$$\mathrm{E}_\gamma = \frac{m_{\chi_1^0}^2 - m_{\tilde{\mathrm{G}}}^2}{2m_{\chi_1^0}}. \tag{5.4}$$

Additionally, the fraction of energy transferred to the photon from the bino is $f_{(DM)} = \mathrm{E}_\gamma/m_{\chi_1^0}$. The physics of energy injection in the decay entirely depends on the lifetime

and the abundance of the parent DM particle, the neutralino. As mentioned by Lucca et al. in Ref. [77], the CMB anisotropies and spectral distortions due to perturbations in the early Universe are complementary and work in two different regions of the parameter space. The parent DM particles with a lifetime between 10^5 s and 10^{12} s mainly affect the thermal history of the Universe before recombination leading to SDs. In contrast, the CMB observables strongly constrain lifetimes between 10^{12} s and 10^{25} s.

The S_8 tension resolution requires a suppression of the linear power spectrum, which induces a change in the sound horizon. The case of decaying dark matter to warm dark matter and dark radiation fulfils the condition mentioned above. However, for the Universe to have the structure we see today, only a fraction of dark matter can decay into WDM. The authors of Ref. [28], provide a model-independent limit on the decay to WDM, which states that with $\epsilon = 0.07\%$, a lifetime of 55 Gyr and the standard ΛCDM parameters the S_8 tension can be solved.

Although this work focuses explicitly on gravitino decay, the physics of the energy injection and coupling constants can be applied to a generic decaying dark matter model.

5.1.1 Results

Spectral distortions and CMB anisotropies can be used to investigate the effects of the decay and the behaviour of particle dark matter. We show a complementary approach to conventional dark matter searches at colliders and experiments. As the popularity of the SUSY and SWIMPs increases in dark matter models, it has become necessary to study and probe a more extensive section of the parameter space for particles. Currently, being weakly coupled, there are few direct/indirect detection bounds on the SWIMP parameter space, and cosmological observations provide the best prospects of probing it.

For our results, we extract the excluded and allowed regions of parameter space for a generic decaying dark matter model from Ref. [77] and, on that impose hypothesised neutralino masses ranging from 10 GeV to 100 TeV. The 100 TeV upper bound arises from the Unitarity limit corresponding to s-wave annihilations for dark matter.

Figure 5.1 shows the excluded and allowed region for a decaying dark matter model, with the fraction of energy transferred to the photon on the y-axis ($f_{(DM)}$) and the lifetime of the parent particle on the x-axis (τ). The plot displays the constraints on the decay, based on present and planned experiments.

- **FIRAS:** The FIRAS (Far InfraRed Absolute Spectrophotomer) the tool was aboard the COBE satellite and measured the difference between the CMB and a perfect blackbody spectrum [13].
- **LiteBird:** LiteBird is a future planned small space observatory that aims to detect signatures of primordial gravitational wave(s) in the form of B-mode polarisation of the CMB [89].
- **CMBS4:** The CMB-S4 is another planned ground-based CMB experiment set to push the boundaries of sensitivity of CMB measurements [90].
- **PRISM:** PRISM was a proposed mission that surveyed the full sky at high resolution and high sensitivity, probing the cosmic history from very early times [91].
- **PIXIE:** PIXIE (Primordial Inflation Explorer) is a future planned experiment to measure the gravity-wave signature of primordial inflation on the linear polarisation of the CMB [14]
- **CMB1 and BBN1:** The labelled CMB1 and BBN1 lines correspond to bounds displayed in figure 5 of Ref. [15].

The coloured regions in Fig. 5.1 are the exclusion parameter spaces based on data from the respectively labelled experiments. The straight lines in the figure labelled as m_χ correspond to the neutralino mass calculated for a range of gravitino masses using Eq. (5.2). For a specified m_χ, every point above the corresponding line also forms a part of the excluded region.

The corresponding decay widths in the SWIMP decay are model-dependent and must be constrained by observations or experiments. Furthermore, these decays are characteristically accompanied by electromagnetic energy release into the cosmic plasma over time scales comparable to the Big Bang Nucleosynthesis and recombination (CMB), which can disrupt the processes. Hence, we can use cosmological probes like spectral distortions, BBN, CMB energy spectrum and CMB anisotropies and any deviations in them to find constraints on generic SWIMP masses and their couplings.

For the energy release to have a significant effect on the thermodynamics of the Universe, there are limitations on the decay widths of the parent particle. Firstly, the lifetime of the parent particle must be shorter than the age of the Universe, which is approximately 10^{17},s. If the lifetime exceeds the age of the Universe, it will be too stable and not decay in abundance. Secondly, for any detectable signatures such as spectral or

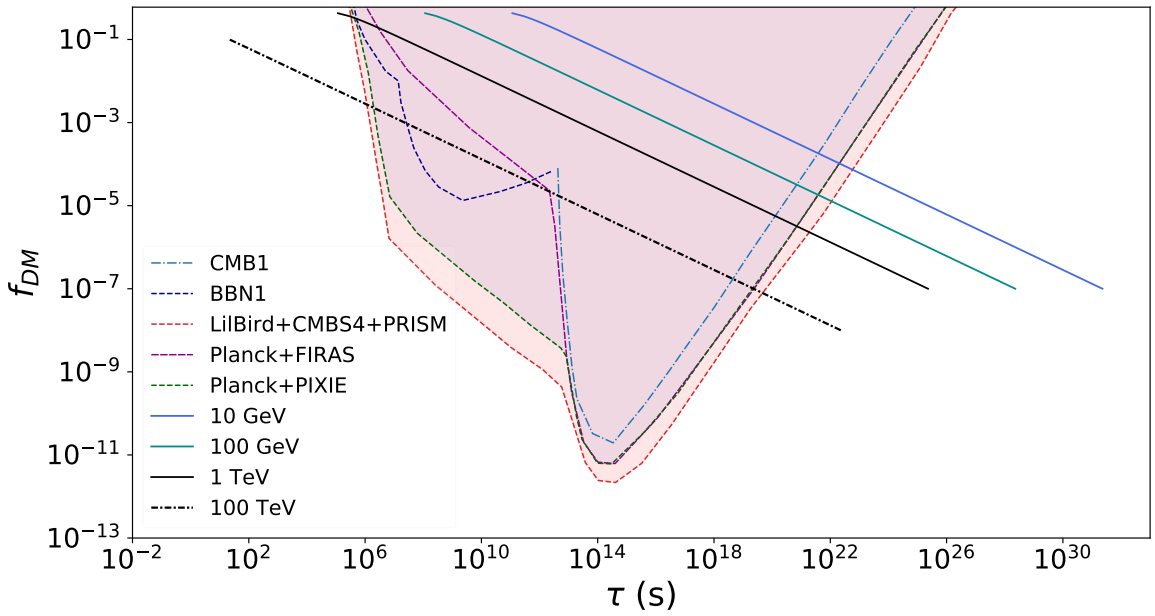

Figure 5.1 Various exclusion regions obtained from observational data for a fraction of the energy injected into the Universe (energy of the photon) vs the lifetime of the parent decaying dark matter particle. The coloured regions are exclusion bounds from current Planck [12], Firas [13] and planned Pixie [14] experiments and the dotted/dash-dotted lines are the bounds imposed by BBN and CMB anisotropies [15]. The linear lines on the plot are for the different valid masses of the neutralino as a parent particle.

CMB distortions to occur, the decay must happen around or just before $10^{11}, \mathrm{s} - 10^{12}$,s. Any earlier decay will not result in detectable signatures.

5.2 Gravitino decay

As a part of this research work, we conducted preliminary investigations for our model's second gravitino decay. We build on the scenario presented in Ref. [76], with a gravitino decaying into a sneutrino and a right-handed neutrino. The authors of Ref. [76] extend the Standard Model by adding a right-handed neutrino to the standard model as a part of the extension to MSSM under the $U(1)B - L$ symmetry. Under this symmetry, the right-handed neutrino can account for the seesaw mechanism and the baryon asymmetry of the Universe with primordial leptogenesis. In addition, this extension to the MSSM allows for freedom of the parameters associated with the lightest right-handed neutrino.

We specifically consider the 100 GeV gravitino case as discussed in Ref. [76], with the sneutrino ($\tilde{\mathrm{N}}_1$) as massive warm dark matter and the right-handed neutrino (N_1) as the massless dark radiation decay product. The physics behind the S_8 resolution mentioned in Ref. [28, 76] is the suppression of the growth of matter fluctuation at $k \sim 0.1 - 1h\mathrm{Mpc}^{-1}$. Similar to the neutralino decay, the decay width of the gravitino can be given as,

$$\Gamma(\tilde{\mathrm{G}} \to \tilde{\mathrm{N}}_1 + \mathrm{N}_1) = \frac{m_{\tilde{\mathrm{G}}}^3}{192\pi M_{\mathrm{Pl}}^2}\left[1 - \left(\frac{m_1}{m_{\tilde{\mathrm{G}}}}\right)\right]^2\left[1 - \left(\frac{m_1}{m_{\tilde{\mathrm{G}}}}\right)^2\right]^3, \tag{5.5}$$

with m_1 as the soft mass of $\tilde{\mathrm{N}}_1$.

The characteristics of the second decay are included in our version of the code, CLASS defined as the two decay parameters Γ and ϵ (Eq. (4.11)). For the resolution of the S_8 tension, according to Ref. [28], the ideal parameter values are $(\Gamma_{\mathrm{CDM}}^{-1}, \epsilon) = (56\,\mathrm{Gyr}, 0.007)$. Using these values, the authors of Ref. [76] claim that the 100 GeV gravitino is an excellent candidate to resolve the S_8 tension. If the mass of the $\tilde{\mathrm{N}}_1$ is predominantly generated through gravity mediation, it makes the sneutrino an ideal candidate for a massive warm dark matter decay product.

5.2.1 Results

We used a different version of ExoCLASS to verify the results of our modified CLASS version for the two-step decay.

We employed our modified version of CLASS to simulate the two-step decay scenario, with the neutralino decay lifetime value of 10^{22}s. A neutralino with a lifetime longer than the age of the Universe (approximately 10^{17}s) would be considered stable and would result in a negligible number of gravitinos. This implies that the majority of the decay dynamics can be captured in the first decay, which is handled by ExoCLASS. To validate our results, we simulated the first decay with the same decay parameters in a separate version of ExoCLASS. The power spectrum residuals from the two codes compared to the Standard Model curve are depicted in Fig. 5.2. The ExoCLASS curve is represented by the blue dashed line, which is nearly identical to the ΛCDM, as expected due to the longer decay lifetime of the neutralino. Our result, represented by the red dashed line, agrees closely until a significant change occurs at higher multipole values. The close agreement of our results with ExoCLASS up to $l \sim 230$, which corresponds to the first

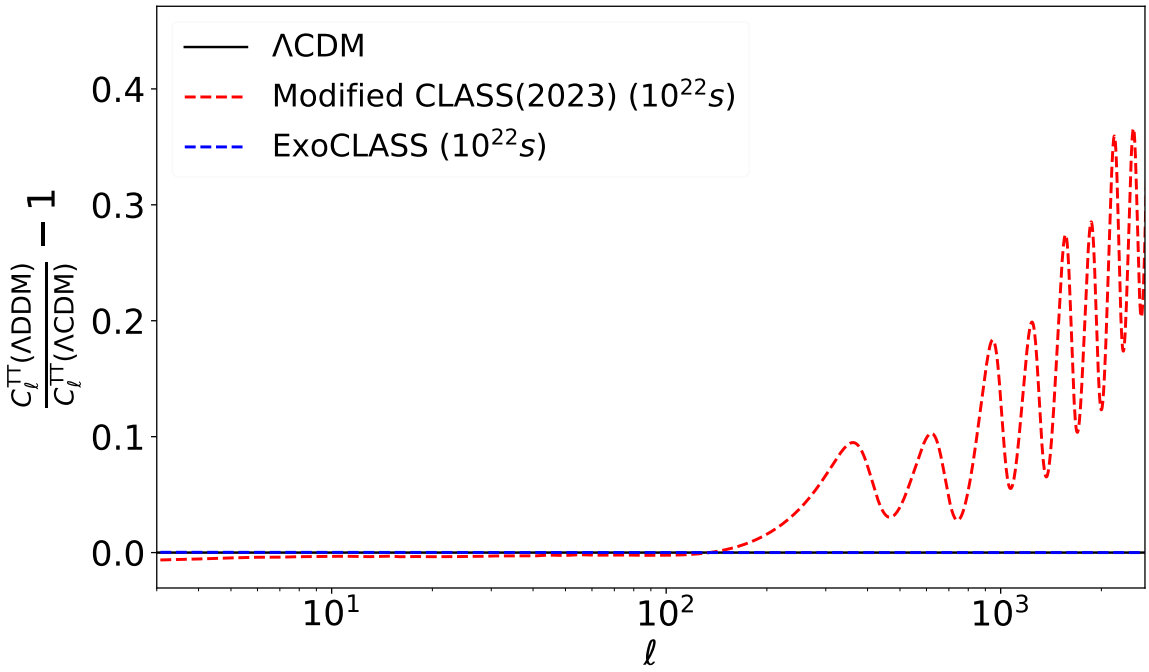

Figure 5.2 A residual plot of CMB temperature power spectrum produced by ExoCLASS and our modified code for the two-step dark matter decay. The solid black line corresponds to the standard ΛCDM, and the blue dashed line is the curve due to neutralino decay as outputted by ExoCLASS. The red dashed line is the curve our modified CLASS version produced for the two-step decay. The decay lifetime for the neutralino is 10^{22} s.

peak in the CMB spectrum, provides a compelling indication that the merged code is functioning properly.

In this work, we also successfully show that cosmological probes, such as CMB anisotropies and spectral distortions can be used to constrain SWIMP masses and their couplings. Additionally, we developed a modified version of the CLASS code capable of handling a decaying dark matter model and its impact on the thermodynamics of the Universe and the ΛCDM model. Although additional research is necessary to test and examine the decay scenario in greater detail, we plan to expand on this work in the future by exploring the properties of decaying dark matter and its ability to address the cosmological tensions. We will also provide an in-depth analysis of the gravitino decay scenario and the two-step decay and share the specifics of the code produced in this study in accompanying publications.

Leading to future work

Lyman-α

The Lyman-α forest power spectrum is an important additional probe of decaying dark matter models typically created to resolve the S_8 tension, which leads to the suppression of the power spectrum on the scales of $k \geq 1h/\text{Mpc}$. The parameter space that addresses the S_8 tension is well compatible with the Lyman-α forest because of suppression of the power spectrum due to the decay builds up at low redshifts [92, 93].

Mathematically, the standard transfer function for WDM can be given as

$$\mathrm{T}(k) = [1 + (\alpha k)^{2v}]^{-5v} \tag{5.6}$$

where α is a parameter encapsulating the dynamical properties of WDM, which can be determined numerically through a Boltzmann code like CLASS. Eq. 5.6 is derived from the estimation calculation for the co-moving particle horizon (since production) with particle velocity $v(t)$,

$$\lambda_{\mathrm{FS}}(t) \simeq \int_{t_{\mathrm{prod}}}^{t} \frac{\mathrm{d}t'}{a(t')} v(t'), \tag{5.7}$$

Fuss et al. [92] investigate a general DCDM to WDM and DR scenario with relation to the Lyman-α forest by using the BOSS-DR14 one-dimensional Lyman-α forest power spectrum [94]. They found that the decay leads to a time-dependent suppression of the CMB power spectrum resulting in lower values of S_8 in the late Universe while still agreeing with the ΛCDM model and its success with the CMB anisotropies and galaxy clustering on the largest scales. Their results confirm that DCDM is a viable candidate for resolving the S_8 tension in agreement with Ref. [28] and our model.

Axino

We can replace the gravitino in our decay with another dark matter candidate, the axino, with the neutralino decaying into an axino and a photon. In this section, we briefly describe the properties of the axino.

The axino is a superpartner of the axion that arises from the strong CP problem of the standard model. The axino, stable or almost stable on cosmological timescales, is considered a well-motivated dark matter candidate. They are extremely weakly interacting (EWIMPs), which gives them different properties to WIMPs and SWIMPs. Relic axinos can be produced in the hot plasma via thermal production mechanisms or via the decays of heavy particles in the early Universe [95].

If produced non-thermally via decays of the NLSP, the axinos couple with the SUSY mother particles with a factor of $1/f_a$, where f_a is the axion decay constant. Like axions, the axino interactions with the SM are suppressed by a factor of f_a. The quantity most relevant to astroparticle physics is the mass of the axino, which has not been widely studied, $m_{\tilde{a}}$. The method to calculate the axino mass is similar to the gravitino mass, related to the goldstino. Recall that the goldstino is the superpartner of the Goldstone boson. Hence, the axino obtains its mass with a similar order of magnitude of the gravitino mass, $m_{3/2}$ [29, 96].

Axinos, although less popular, are electrically and colour neutral making them an interesting candidate for dark matter. Considering the neutralino as the parent particle, we can define the relic density of axinos similar to the relic density of gravitinos,

$$\Omega_{\tilde{a}} \simeq \frac{m_{\tilde{a}}}{m_{\rm WIMP}} \Omega_{\rm WIMP} \simeq 2.7 \times 10^{10} \left(\frac{m_{\tilde{a}}}{100\,{\rm GeV}} \right) Y_{\rm WIMP}, \tag{5.8}$$

where $Y_{\rm WIMP}$ is the WIMP abundance.

The axino-specific case, along with Lyman-α forest constraints, will be explored in detail in our accompanying paper that will be released in the near future.

Chapter 6

Conclusion & Future Work

The standard model of cosmology is a well-accepted paradigm for studying the Universe. Many experiments so far have been able to measure and identify a variety of observables that describe our Universe. Results of early and late time Universe measurements have revealed multiple tensions in the parameters of the ΛCDM model. In light of these potential anomalies, researchers have set out in search of new physics in the hopes of finding resolutions for the tensions.

The existence of the dark sector in the Universe has initiated a multitude of theories about its role in the evolution of the Universe and its potential to solve any cosmological tensions. Such approaches explore the potential diversity in the dark sector, which may be similar to the one in the standard model of particle physics. In addition, there is active research on decaying dark matter and its explanation for some of the phenomena observed in the Universe.

This thesis presents details of work performed to study the phenomenology of a decaying dark matter model to resolve the popular S_8 and H_0 cosmological tensions. We achieved this by focusing on the interplay between the Standard Model of particle physics and its supersymmetric extension, with supersymmetric candidates for dark matter, which are introduced in Chapter 1. We build on existing decaying dark matter literature and present a two-step decay model with a combination of cold and warm dark matter decay products.

Chapter 2 details the timeline of key events in the history of the Universe. The history of the Universe is the backbone for understanding the characteristics and effects of dark matter decay at different periods in the evolution of the Universe. Additionally, the Universe is parametrized by the most popular and well-rounded Big Bang cosmological

model, the ΛCDM model, also known as the standard cosmological model. The Standard Model of cosmology and its parameters in Chapter 3. Its parameters and observation of the cosmic microwave background, also detailed in Chapter 3, form the basis of any model-building and calculation of beyond-standard-model physics, such as decaying dark matter.

As a significant part of this research work, we successfully modified a public Boltzmann code, CLASS, to accommodate our two-step decaying dark matter model consisting of cold and warm dark matter. A comprehensive guide to the methodology of our changes and the code performance is presented in Chapter 4. In addition, this work presents computational and physical verification of the results obtained from the code by appropriate comparisons to current published literature. Our results agree with popular findings that decaying dark matter into warm dark matter can resolve the S_8 tension, although not the H_0 tension.

On our path to investigating the complete two-step decay and its effects on the CMB observables, we point out that cosmological observations can provide excellent constraints on supersymmetric SuperWIMPs. For example, the CMB energy spectrum, the CMB temperature and polarisation anisotropies, and the observed light element abundances provide stringent constraints on the SuperWIMP parameter space, complementary to the SUSY collider dark matter searches and indirect or direct dark matter experiments. We provide details of cosmological constraints and our results of our decay model in Chapter 5.

Overall, we have successfully defined all components of a decaying dark matter model, providing an accompanying modified Boltzmann code and a new method of probing SuperWIMP parameter space through cosmological observations. In the future, we see several avenues for improvement and further extension of our decaying dark matter framework. One such avenue is to consider other dark matter candidates, such as the axion instead of the gravitino. Additionally, a complete investigation of a general two-step dark matter decay is in progress, with Monte-Carlo simulations. Finally, a paper detailing the cosmological constraints on SuperWIMPs and another accompanying our modified code will be published in the near future. We conclude this work by showing that research into decaying dark matter phenomenology and cosmological probes to study WIMP/SuperWIMP behaviour, can advance our understanding of the structure of the Universe and allow a peek into its secrets.

Appendix

In this section, we have presented the input file we used to develop, test and verify our modified version of CLASS and produce the results as shown in Fig.5.2. The parameters are defined in Chapter 4 of this thesis. For a detailed description for each parameter refer to CLASS documentation Ref. [31].

```
write warnings = yes
write background = yes
write parameters = yes

root                    = output/results_1_
DM_mass                 = 100
tau_dcdm_exo            = 2e+22 #seconds
decay_fraction          = 1e-8
photon_energy           = 1e-6 #GeV


------------------L C D M parameters-------------------------------
n_s                     = 0.9673
A_s                     = 2.215e-9
H0                      = 67.70
z_reio                  = 8.24
omega_b                 = 0.022032
T_cmb                   = 2.7255
omega_cdm               = 0.001
recombination           = HyRec
N_ur                    = 2.0328
```

```
------------------1st Decay-----------------------------------------
---> ExoCLASS (DarkAges)
test_param                          = 1
on the spot                         = no
energy_deposition_function          = DarkAges
DarkAges_mode                       = built_in
energy_repartition_coefficient      = no_factorization

injected_particle_spectra           = dirac_photon
injected_particle_branching_ratio = 1

------------------2nd Decay-----------------------------------------
omega_dcdmdrwdm                 = 0.12038
M_dcdm                          = 1
N_ncdm                          = 2
background_ncdm_distribution = 0, 1
m_ncdm                          = 0.06, 0
Gamma_dcdm_wdm                  = 1e-10
epsilon_dcdm_wdm                = 0.0067

----------------Default CLASS parameters-----------------------------
output                  = tCl, pCl, lCl, mPk
lensing                 = yes
l_max_scalars           = 2600
z_pk                    = 0,3
P_k_max_h/Mpc           = 1.0
z_max_pk                = 4.0
k_output_values         = 0.001, 0.01, 0.1, 1
evolver                 = 0

input_verbose = 1
background_verbose = 1
thermodynamics_verbose = 1
perturbations_verbose = 1
transfer_verbose = 1
primordial_verbose = 1
```

```
spectra_verbose = 1
nonlinear_verbose = 1
lensing_verbose = 1
output_verbose = 1
```

Bibliography

[1] "Standard model." https://en.wikipedia.org/wiki/Standard_Model. (document), 1.1

[2] "Supersymmetry taking a closer look at lhc." https://www.lhc-closer.es/taking_a_closer_look_at_lhc/0.supersymmetry. (document), 1.2

[3] M. Battaglieri et al., *US Cosmic Visions: New Ideas in Dark Matter 2017: Community Report*, in *U.S. Cosmic Visions: New Ideas in Dark Matter*, 7, 2017. arXiv:1707.04591. (document), 1.3

[4] A. Belenchia, M. Carlesso, Ömer Bayraktar, D. Dequal, I. Derkach, G. Gasbarri et al., *Quantum physics in space*, *Physics Reports* **951** (2022) 1–70. (document), 1.3

[5] N. Polukhina and N. Starkov, *New experiment for wimp direct search (newsdm)*, *EPJ Web of Conferences* **191** (01, 2018) 02023. (document), 1.4, 1.5.2

[6] A. Ferrantelli, *Gravitino phenomenology and cosmological implications of supergravity*, other thesis, 2, 2010. (document), 2.1

[7] D. Hooper, *Particle Dark Matter*, in *Theoretical Advanced Study Institute in Elementary Particle Physics: The Dawn of the LHC Era*, pp. 709–764, 2010. arXiv:0901.4090. DOI. (document), 2.2

[8] "Dark matter densities." https://www.particlebites.com/?p=7004. (document), 2.2

[9] E. W. Kolb and M. S. Turner, *The Early Universe*, vol. 69. 1990, 10.1201/9780429492860. (document), 2.2, 3.2.1

[10] K. Freese, *Review of observational evidence for dark matter in the universe and in upcoming searches for dark stars*, *EAS Publications Series* **36** (2009) 113–126.

(document), 2.3

[11] "Cmb images." https://www.esa.int/ESA_Multimedia/Images/2013/03/Planck_CMB. (document), 3.1

[12] Planck collaboration, N. Aghanim et al., *Planck 2018 results. I. Overview and the cosmological legacy of Planck*, *Astron. Astrophys.* **641** (2020) A1, [arXiv:1807.06205]. (document), 3.2, 3.3, 3.1, 4.2, 4.7, 5.1

[13] D. J. Fixsen, E. S. Cheng, J. M. Gales, J. C. Mather, R. A. Shafer and E. L. Wright, *The Cosmic Microwave Background spectrum from the full COBE FIRAS data set*, *Astrophys. J.* **473** (1996) 576, [astro-ph/9605054]. (document), 5.1.1, 5.1

[14] A. Kogut, D. Fixsen, D. Chuss, J. Dotson, E. Dwek, M. Halpern et al., *The primordial inflation explorer (pixie): a nulling polarimeter for cosmic microwave background observations*, *Journal of Cosmology and Astroparticle Physics* **2011** (2011) 025. (document), 5.1.1, 5.1

[15] V. Poulin, J. Lesgourgues and P. D. Serpico, *Cosmological constraints on exotic injection of electromagnetic energy*, *JCAP* **03** (2017) 043, [arXiv:1610.10051]. (document), 4.6, 5.1.1, 5.1

[16] "History of cosmology." http://abyss.uoregon.edu/~js/ast123/lectures/lec01.html. (document)

[17] A. A. Penzias and R. W. Wilson, *A Measurement of excess antenna temperature at 4080-Mc/s*, *Astrophys. J.* **142** (1965) 419–421. (document)

[18] WMAP collaboration, D. N. Spergel et al., *First year Wilkinson Microwave Anisotropy Probe (WMAP) observations: Determination of cosmological parameters*, *Astrophys. J. Suppl.* **148** (2003) 175–194, [astro-ph/0302209]. (document)

[19] A. G. Riess, S. Casertano, W. Yuan, J. B. Bowers, L. Macri, J. C. Zinn et al., *Cosmic Distances Calibrated to 1% Precision with Gaia EDR3 Parallaxes and Hubble Space Telescope Photometry of 75 Milky Way Cepheids Confirm Tension with ΛCDM*, *Astrophys. J. Lett.* **908** (2021) L6, [arXiv:2012.08534]. (document)

[20] HST collaboration, W. L. Freedman et al., *Final results from the Hubble Space Telescope key project to measure the Hubble constant*, *Astrophys. J.* **553** (2001) 47–72, [astro-ph/0012376]. (document)

[21] A. G. Riess et al., *A Comprehensive Measurement of the Local Value of the Hubble Constant with 1 km s Mpc Uncertainty from the Hubble Space Telescope and the SH0ES Team*, *Astrophys. J. Lett.* **934** (2022) L7, [arXiv:2112.04510]. (document)

[22] E. Di Valentino, O. Mena, S. Pan, L. Visinelli, W. Yang, A. Melchiorri et al., *In the realm of the Hubble tension—a review of solutions*, *Class. Quant. Grav.* **38** (2021) 153001, [arXiv:2103.01183]. (document)

[23] E. Di Valentino et al., *Cosmology intertwined III: $f\sigma_8$ and S_8*, *Astropart. Phys.* **131** (2021) 102604, [arXiv:2008.11285]. (document)

[24] E. Abdalla et al., *Cosmology intertwined: A review of the particle physics, astrophysics, and cosmology associated with the cosmological tensions and anomalies*, *JHEAp* **34** (2022) 49–211, [arXiv:2203.06142]. (document)

[25] J. L. Feng, A. Rajaraman and F. Takayama, *SuperWIMP dark matter signals from the early Universe*, *Phys. Rev. D* **68** (2003) 063504, [hep-ph/0306024]. (document), 4, 5

[26] S. P. Martin, *A Supersymmetry primer*, *Adv. Ser. Direct. High Energy Phys.* **18** (1998) 1–98, [hep-ph/9709356]. (document), 1.2, 1.2, 1.3, 1.3.1, 1.5.1, 1.5.1, 2.2

[27] M. Bolz, A. Brandenburg and W. Buchmuller, *Thermal production of gravitinos*, *Nucl. Phys. B* **606** (2001) 518–544, [hep-ph/0012052]. (document)

[28] G. Franco Abellán, R. Murgia and V. Poulin, *Linear cosmological constraints on two-body decaying dark matter scenarios and the S8 tension*, *Phys. Rev. D* **104** (2021) 123533, [arXiv:2102.12498]. (document), 4.4.1, 4.4.1, 4.4.1, 4.4.1, 4.6, 4.7, 4.7, 4.8, 5.1, 5.2, 5.2, 5.2.1

[29] F. D. Steffen, *Dark Matter Candidates - Axions, Neutralinos, Gravitinos, and Axinos*, *Eur. Phys. J. C* **59** (2009) 557–588, [arXiv:0811.3347]. (document), 5.2.1

[30] V. Poulin, P. D. Serpico and J. Lesgourgues, *A fresh look at linear cosmological constraints on a decaying dark matter component*, *JCAP* **08** (2016) 036, [arXiv:1606.02073]. (document)

[31] J. Lesgourgues, *The Cosmic Linear Anisotropy Solving System (CLASS) I: Overview*, arXiv:1104.2932. (document), 4.1, 4.8

[32] G. Franco Abellán, R. Murgia, V. Poulin and J. Lavalle, *Implications of the S_8 tension for decaying dark matter with warm decay products*, *Phys. Rev. D* **105**

(2022) 063525, [arXiv:2008.09615]. (document), 4, 4.4

[33] H. Liu, G. W. Ridgway and T. R. Slatyer, *Code package for calculating modified cosmic ionization and thermal histories with dark matter and other exotic energy injections*, *Phys. Rev. D* **101** (2020) 023530, [arXiv:1904.09296]. (document)

[34] J. Chluba and R. A. Sunyaev, *The evolution of CMB spectral distortions in the early Universe*, *Mon. Not. Roy. Astron. Soc.* **419** (2012) 1294–1314, [arXiv:1109.6552]. (document), 4.2

[35] M. Maerker, *Search for heavy neutral Higgs bosons decaying into the fully hadronic di-tau final state with ATLAS*. PhD thesis, Technische Universität Dresden, Institut für Kern- und Teilchenphysik, TU, Dresden (main), 2021. 1, 1.2, 1.3, 1.3.1

[36] M. K. Gaillard, P. D. Grannis and F. J. Sciulli, *The Standard model of particle physics*, *Rev. Mod. Phys.* **71** (1999) S96–S111, [hep-ph/9812285]. 1.1, 1.1

[37] M. D. Schwartz, *Quantum Field Theory and the Standard Model*. Cambridge University Press, 3, 2014. 1.1

[38] C. Giganti, S. Lavignac and M. Zito, *Neutrino oscillations: The rise of the pmns paradigm*, *Progress in Particle and Nuclear Physics* **98** (2018) 1–54. 1.1

[39] M. E. Peskin and D. V. Schroeder, *An Introduction to quantum field theory*. Addison-Wesley, Reading, USA, 1995. 1.1.1

[40] P. W. Higgs, *Broken Symmetries and the Masses of Gauge Bosons*, *Phys. Rev. Lett.* **13** (1964) 508–509. 1.2

[41] F. Englert and R. Brout, *Broken Symmetry and the Mass of Gauge Vector Mesons*, *Phys. Rev. Lett.* **13** (1964) 321–323. 1.2

[42] I. Melo, *Higgs potential and fundamental physics*, *Eur. J. Phys.* **38** (2017) 065404, [arXiv:1911.08893]. 1.2

[43] T. Markkanen, A. Rajantie and S. Stopyra, *Cosmological aspects of higgs vacuum metastability*, *Frontiers in Astronomy and Space Sciences* **5** (2018) . 1.2

[44] J. Oliver, *Search for Supersymmetric Electroweak Production and the Measurement of Higgs Production Cross-sections at the ATLAS Experiment*. PhD thesis, Adelaide U., 2020. 1.3.1

[45] G. Bertone and D. Hooper, *History of dark matter*, *Rev. Mod. Phys.* **90** (2018)

045002, [arXiv:1605.04909]. 1.4, 2.2

[46] WMAP collaboration, E. Komatsu et al., *Five-Year Wilkinson Microwave Anisotropy Probe (WMAP) Observations: Cosmological Interpretation*, *Astrophys. J. Suppl.* **180** (2009) 330–376, [arXiv:0803.0547]. 1.4

[47] K. Garrett and G. Duda, *Dark Matter: A Primer*, *Adv. Astron.* **2011** (2011) 968283, [arXiv:1006.2483]. 1.4, 1.4.1, 2.1, 2.1, 2.2

[48] R. Catena and L. Covi, *SUSY dark matter(s)*, *Eur. Phys. J. C* **74** (2014) 2703, [arXiv:1310.4776]. 1.4.1, 2.2

[49] L. Hsu, "Particle-like Dark Matter." ICHEP 2020 Plenary talk, Prague, 2020. 1.4.1

[50] J. Billard et al., *Direct detection of dark matter—APPEC committee report**, *Rept. Prog. Phys.* **85** (2022) 056201, [arXiv:2104.07634]. 1.4.1

[51] J. L. Feng, *Supersymmetry and cosmology*, *eConf* **C0307282** (2003) L11, [hep-ph/0405215]. 1.5.2, 1.5.2, 1.5.2

[52] J. L. Feng, S. Su and F. Takayama, *Supergravity with a gravitino LSP*, *Phys. Rev. D* **70** (2004) 075019, [hep-ph/0404231]. 1.5.2, 4.2

[53] G. F. Giudice, A. Riotto and I. Tkachev, *Thermal and nonthermal production of gravitinos in the early Universe*, *JHEP* **11** (1999) 036, [hep-ph/9911302]. 1.5.2

[54] C. Autermann, *Experimental status of supersymmetry after the LHC Run-I*, *Prog. Part. Nucl. Phys.* **90** (2016) 125–155, [arXiv:1609.01686]. 1.5.2

[55] GAMBIT collaboration, P. Athron et al., *Combined collider constraints on neutralinos and charginos*, *Eur. Phys. J. C* **79** (2019) 395, [arXiv:1809.02097]. 1.5.2

[56] B. Fuks, M. Klasen, D. R. Lamprea and M. Rothering, *Revisiting slepton pair production at the Large Hadron Collider*, *JHEP* **01** (2014) 168, [arXiv:1310.2621]. 1.5.2

[57] C. A. J. O'Hare, *New definition of the neutrino floor for direct dark matter searches*, *Phys. Rev. Lett.* **127** (Dec, 2021) 251802. 1.5.2

[58] "Neutrino floor." https://www.symmetrymagazine.org/article/september-2015/hitting-the-neutrino-floor. 1.5.2

[59] M. Peskin, "Supersymmetric dark matter in the harsh light of the Large Hadron Collider." Particle Physics and Astrophysics Division, SLAC, Stanford University, 2013. 1.5.2

[60] V. Mukhanov, *Physical Foundations of Cosmology*. Cambridge University Press, Oxford, 2005, 10.1017/CBO9780511790553. 2.1, 2.1

[61] S. Dodelson, *Modern Cosmology*. Academic Press, Amsterdam, 2003. 2.1, 2.1, 2.1, 2.1, 3.1, 4.1

[62] D. Baumann, *Cosmology, Lecture Notes*. Department of Applied Mathematics and Theoretical Physics, University of Cambridge, NA. 2.1, 2.1, 2.1, 2.1, 2.2, 3.1, 3.1, 3.1, 3.1, 3, 4.1

[63] A. H. Jaffe, *Cosmology 2012: Lecture notes*, 2012. 2.1, 3.1, 3.1, 3.1, 3.1

[64] V. C. Rubin and W. K. Ford, Jr., *Rotation of the Andromeda Nebula from a Spectroscopic Survey of Emission Regions*, *Astrophys. J.* **159** (1970) 379–403. 2.2

[65] L. Bergström, *Cosmology and the Dark Matter Frontier*, *Phys. Scripta T* **158** (2013) 014014, [arXiv:1309.7267]. 2.2

[66] D. Lincoln and B. Nord, *The Expanding Universe: Dark Energy*, *Phys. Teacher* **52** (2014) 337–343. 2.2

[67] M. P. Hobson, G. P. Efstathiou and A. N. Lasenby, *General relativity: An introduction for physicists*. 2006. 3.1

[68] L. Bergström, *Multi-Messenger Astronomy and Dark Matter*, in *40th Saas-Fee Course: Astrophysics at Very-High Energies*, Saas-Fee Advanced Course, pp. 123–222, 2013. arXiv:1202.1170. DOI. 3.1

[69] M. Bauer and T. Plehn, *Yet Another Introduction to Dark Matter: The Particle Physics Approach*, vol. 959 of *Lecture Notes in Physics*. Springer, 2019, 10.1007/978-3-030-16234-4. 3.2

[70] W. Hu and S. Dodelson, *Cosmic Microwave Background Anisotropies*, *Ann. Rev. Astron. Astrophys.* **40** (2002) 171–216, [astro-ph/0110414]. 3.2.1, 3.2.2

[71] "Notes on cmb." http://www.quantumfieldtheory.info/cmb_vers_2.pdf. 3.2.1

[72] K. N. Abazajian et al., *Inflation Physics from the Cosmic Microwave Background and Large Scale Structure*, *Astropart. Phys.* **63** (2015) 55–65, [arXiv:1309.5381].

3.2.2

[73] H. D. Poulter, *Investigating the Effect of Primordial Black Hole Hawking Radiation on the Cosmic Microwave Background*. PhD thesis, Adelaide U., 2018. 3.2.2

[74] R. K. Sachs and A. M. Wolfe, *Perturbations of a cosmological model and angular variations of the microwave background*, *Astrophys. J.* **147** (1967) 73–90. 3.2.2

[75] W. Hu, *CMB temperature and polarization anisotropy fundamentals*, *Annals Phys.* **303** (2003) 203–225, [astro-ph/0210696]. 3.2.3

[76] G. Choi and T. T. Yanagida, *Gravitino cosmology helped by a right handed (s)neutrino*, *Physics Letters B* **827** (2022) 136954. 4, 4.4, 5, 5.2, 5.2

[77] M. Lucca, N. Schöneberg, D. C. Hooper, J. Lesgourgues and J. Chluba, *The synergy between CMB spectral distortions and anisotropies*, *JCAP* **02** (2020) 026, [arXiv:1910.04619]. 4, 4.6, 5.1, 5.1.1

[78] U. Seljak and M. Zaldarriaga, "CMBFAST: A microwave anisotropy code." Astrophysics Source Code Library, record ascl:9909.004, Sept., 1999. 4.1

[79] A. Lewis and A. Challinor, "CAMB: Code for Anisotropies in the Microwave Background." Astrophysics Source Code Library, record ascl:1102.026, Feb., 2011. 4.1

[80] S. Seager, D. D. Sasselov and D. Scott, *A new calculation of the recombination epoch*, *Astrophys. J. Lett.* **523** (1999) L1–L5, [astro-ph/9909275]. 4.1

[81] Y. Ali-Haïmoud and C. M. Hirata, *HyRec: A fast and highly accurate primordial hydrogen and helium recombination code*, *Physical Review D* **83** (feb, 2011) . 4.1

[82] "Acoustic peaks." https://ned.ipac.caltech.edu/level5/Sept02/Reid/Reid5_2.html. 4.1

[83] P. Stöcker, M. Krämer, J. Lesgourgues and V. Poulin, *Exotic energy injection with ExoCLASS: Application to the Higgs portal model and evaporating black holes*, *JCAP* **03** (2018) 018, [arXiv:1801.01871]. 4.2, 4.3, 4.3, 4.6, 4.8

[84] J. L. Feng, *Dark Matter Candidates from Particle Physics and Methods of Detection*, *Ann. Rev. Astron. Astrophys.* **48** (2010) 495–545, [arXiv:1003.0904]. 4.2

[85] T. R. Slatyer, N. Padmanabhan and D. P. Finkbeiner, *CMB Constraints on WIMP Annihilation: Energy Absorption During the Recombination Epoch*, *Phys. Rev. D*

80 (2009) 043526, [arXiv:0906.1197]. 4.3

[86] M. Cirelli, G. Corcella, A. Hektor, G. Hutsi, M. Kadastik, P. Panci et al., *PPPC 4 DM ID: A Poor Particle Physicist Cookbook for Dark Matter Indirect Detection*, *JCAP* **03** (2011) 051, [arXiv:1012.4515]. 4.3

[87] C.-P. Ma and E. Bertschinger, *Cosmological perturbation theory in the synchronous and conformal Newtonian gauges*, *Astrophys. J.* **455** (1995) 7–25, [astro-ph/9506072]. 4.4.1, 4.4.1

[88] S. Aoyama, T. Sekiguchi, K. Ichiki and N. Sugiyama, *Evolution of perturbations and cosmological constraints in decaying dark matter models with arbitrary decay mass products*, *JCAP* **07** (2014) 021, [arXiv:1402.2972]. 4.4.1

[89] LiteBIRD collaboration, Y. Sekimoto et al., *Concept Design of Low Frequency Telescope for CMB B-mode Polarization satellite LiteBIRD*, *Proc. SPIE Int. Soc. Opt. Eng.* **11453** (2020) 1145310, [arXiv:2101.06342]. 5.1.1

[90] CMB-S4 collaboration, K. Abazajian et al., *CMB-S4: Forecasting Constraints on Primordial Gravitational Waves*, *Astrophys. J.* **926** (2022) 54, [arXiv:2008.12619]. 5.1.1

[91] PRISM collaboration, P. André et al., *PRISM (Polarized Radiation Imaging and Spectroscopy Mission): An Extended White Paper*, *JCAP* **02** (2014) 006, [arXiv:1310.1554]. 5.1.1

[92] L. Fuss and M. Garny, *Decaying Dark Matter and Lyman-α forest constraints*, arXiv:2210.06117. 5.2.1, 5.2.1

[93] W. B. Lin, D. H. Huang, X. Zhang and R. H. Brandenberger, *Nonthermal production of WIMPs and the subgalactic structure of the Universe*, *Phys. Rev. Lett.* **86** (2001) 954, [astro-ph/0009003]. 5.2.1

[94] M. Blomqvist et al., *Baryon acoustic oscillations from the cross-correlation of Lyα absorption and quasars in eBOSS DR14*, *Astron. Astrophys.* **629** (2019) A86, [arXiv:1904.03430]. 5.2.1

[95] K.-Y. Choi, L. Covi, J. E. Kim and L. Roszkowski, *Axino Cold Dark Matter Revisited*, *JHEP* **04** (2012) 106, [arXiv:1108.2282]. 5.2.1

[96] K.-Y. Choi, J. E. Kim and L. Roszkowski, *Review of axino dark matter*, *J. Korean Phys. Soc.* **63** (2013) 1685–1695, [arXiv:1307.3330]. 5.2.1